

## Nonmesonic weak decay of $\Lambda$ hypernuclei: The $\Lambda N$ - $\Sigma N$ coupling

E. Bauer,<sup>1,2,\*</sup> G. Garbarino,<sup>3</sup> and C. A. Rodríguez Peña<sup>2,4</sup>

<sup>1</sup>*Facultad de Ciencias Astronómicas y Geofísicas, Universidad Nacional de La Plata, Argentina*

<sup>2</sup>*IFLP, CONICET, C.C. 67, 1900 La Plata, Argentina*

<sup>3</sup>*IIS G. Peano, I-10125 Torino, Italy*

<sup>4</sup>*Departamento de Física, Universidad Nacional de La Plata, La Plata, Argentina*

(Received 16 June 2017; revised manuscript received 17 August 2017; published 5 October 2017)

The nonmesonic weak decay of  $\Lambda$  hypernuclei is studied within a microscopic diagrammatic approach which is extended to include the  $\Lambda N$ - $\Sigma N$  strong interaction coupling. We adopt a nuclear matter formalism which, through the local density approximation, allows us to model finite hypernuclei. One-meson-exchange potentials are used for the weak and strong four-baryon interactions. The rates for the neutron- and proton-induced weak decays,  $\Lambda N \rightarrow nN$  and  $\Lambda N \rightarrow \Sigma N \rightarrow nN$  ( $N = n$  or  $p$ ;  $\Sigma = \Sigma^-, \Sigma^0$ , and  $\Sigma^+$ ), are predicted for  ${}_{\Lambda}^{12}\text{C}$ ,  ${}_{\Lambda}^{28}\text{Si}$ ,  ${}_{\Lambda}^{56}\text{Fe}$ , and  ${}_{\Lambda}^{208}\text{Pb}$ . The  $\Lambda N$ - $\Sigma N$  coupling turns out to provide a contribution of about 23% (5%) to the total neutron-induced rate (proton-induced rate). Again as an effect of the hyperon coupling, the total one-nucleon-induced rate increases by about 9%, while the  $\Gamma_n/\Gamma_p$  ratio increases by about 17%. The saturation property of the nonmesonic rates with increasing hypernuclear mass number is clearly obtained and explained. The above percentage modifications remain almost unaltered through the hypernuclear mass number. All the non-negligible changes introduced by the  $\Lambda N$ - $\Sigma N$  coupling lead to a definite improvement of our predictions once compared with the available KEK and FINUDA data.

DOI: [10.1103/PhysRevC.96.044303](https://doi.org/10.1103/PhysRevC.96.044303)

### I. INTRODUCTION

Hypernuclei containing a  $\Lambda$  baryon are produced in the ground state or in an excited state of the  $\Lambda$ -particle neutron-hole configuration. When a  $\Lambda$  hypernucleus is excited above the particle emission threshold it decays dominantly by the strong interaction, through nucleon or cluster emission. The remaining strange nuclear system then deexcites to its ground state via electromagnetic transitions. A  $\Lambda$  hypernucleus in the ground state is stable at the nuclear time scale ( $\sim 10^{-23}$  s) and thus can only decay to nonstrange nuclear systems, via weak interaction processes, which are by far slower. These strangeness-changing processes can take place in two different ways. The mesonic mode,  $\Lambda \rightarrow \pi N$ , resembles what happens to the  $\Lambda$  in free space, but is increasingly suppressed in hypernuclei due to the Pauli principle as the mass number increases. The nonmesonic mode, with channels  $\Lambda N \rightarrow nN$ ,  $\Lambda NN \rightarrow nNN$ , etc, can only occur in nuclear systems, and provides an invaluable tool for investigating weak baryon interactions. The nonmesonic mode dominates over the mesonic mode for all but the  $s$ -shell hypernuclei, and only for very light systems ( $A \leq 5$ ) are the two decay modes competitive.

After more than 60 years from its inception, hypernuclear physics is a mature field of research [1] which in many aspects is located at the crossroads between hadronic and nuclear physics. It implies important connections with QCD and with dense astrophysical objects. This is true, in particular, for the nonmesonic hypernuclear weak decay [2]. The equilibrium between  $NN \rightarrow \Lambda N$  and  $\Lambda N \rightarrow NN$  nonmesonic weak processes is expected to be extremely important for explaining the stability of rotating neutron stars with respect to the emission of gravitational waves. The fundamental property which controls the stability of a neutron star is the viscosity,

which dominantly depends on nonmesonic weak processes involving hyperons. Other related hyperon-induced weak interactions (the so-called Urca processes) provide a relevant contribution to the cooling mechanism of neutron stars. The occurrence of hyperon superfluidity is indispensable for this hyperon cooling scenario to be consistent with the observations on cold neutron stars.

Nowadays, a more than satisfactory consensus has been reached between the theoretical description and experiments on the mesonic decay. Concerning the nonmesonic decay, we recall that the innovative experiments performed in the last 20 years or so and the advent of elaborated theoretical models allowed us to reach a reasonable agreement between data and predictions for the total and partial nonmesonic rates—especially the ratio  $\Gamma_n/\Gamma_p \equiv \Gamma(\Lambda n \rightarrow nn)/\Gamma(\Lambda p \rightarrow np)$  between the neutron- and the proton-induced decay rates and the two-nucleon-induced decay rate  $\Gamma_2$ —and the intrinsic asymmetry parameter for the decay of polarized hypernuclei. Complete reviews of the experimental results and the theoretical approaches on these issues can be found in [1,3].

It is widely recognized that the so-called  $\Gamma_n/\Gamma_p$  and asymmetry puzzles have been satisfactorily resolved. However, the relatively large experimental error bars still do not allow us to discriminate between various proposed weak interaction schemes. Moreover, discrepancies between theory and experiment (and in some case even between different experiments) are still present for the emission spectra involving protons. This could signal an imperfect implementation of final state interaction effects in the theoretical and/or experimental analysis or the relevance of other theoretically unknown mechanisms. For instance, it is still unclear what role is played in the nonmesonic decay by possible violations of the  $\Delta I = 1/2$  rule on the isospin change. Nowadays, no experimental indication supports or excludes the validity of this rule for the weak couplings of the  $\Lambda$  hyperon with

\*Corresponding author: [bauer@fisica.unlp.edu.ar](mailto:bauer@fisica.unlp.edu.ar)

mesons heavier than the pion in the  $\Lambda N \rightarrow nN$  processes. In particular, the quality of present data on the one-nucleon-induced nonmesonic weak decay prevents us from extracting the effect of  $\Delta I = 3/2$  terms. New and more precise experiments are necessary (for details on the status concerning this issue see the first review paper in [1]). A detailed description of the hyperon weak interactions underlying hypernuclear decay is thus impossible at present. From the theoretical viewpoint, given the aforementioned discrepancies between theory and hypernuclear data, new decay mechanisms should be explored.

Another aspect which deserves further attention concerns the relevance of the  $\Lambda N$ - $\Sigma N$  strong coupling on the non-mesonic weak decay. This interaction mechanism, which we study in this contribution, introduces, besides the well known nonmesonic decay channels  $\Lambda N \rightarrow nN$ , new, second-order processes  $\Lambda N \rightarrow \Sigma N \rightarrow nN$ . The strong interaction coupling between  $\Lambda N$  and  $\Sigma N$  states (analogously, among  $\Lambda\Lambda$ ,  $\Xi N$ , and  $\Sigma\Sigma$  states for multistrangeness systems) has proven to be important to understand the structure of  $\Lambda$  hypernuclei (double- $\Lambda$  and  $\Xi$  hypernuclei) and in studies of dense stars. One can interpret the  $\Lambda N$ - $\Sigma N$  baryon coupling as a source of a  $\Sigma$  admixture in  $\Lambda$  hypernuclear states, i.e., a virtual excitation of the  $\Lambda$  into a  $\Sigma$ . We summarize in the following paragraphs the current knowledge on the influence of this coupling on the structure of  $\Lambda$  hypernuclei and later we return to the issue of the nonmesonic weak decay.

The  $\Lambda NN$  strong three-body interaction was revealed to be an important ingredient to investigate the structure of  $\Lambda$  hypernuclei [4], especially for light systems [5]. This interaction turned out to be crucial to solve the so-called overbinding problem concerning  $s$ -shell hypernuclei. In particular, the relevant part of the  $\Lambda NN$  interaction is the one which is induced by the  $\Lambda N$ - $\Sigma N$  strong coupling, which also leads to a non-negligible second-order tensor force in the  $\Lambda N$  strong interaction. Effects of the coupling between  $\Lambda N$  and  $\Sigma N$  states are also found in hypernuclei with a neutron excess [6] and possibly in the composition and the equation of state of neutron stars [7]. In hypernuclei, the coupling to intermediate  $\Sigma N$  states in the  $\Lambda N$  strong interaction is more important—especially because of the relatively small  $\Sigma$ - $\Lambda$  mass difference,  $m_\Sigma - m_\Lambda \sim 78$  MeV—than the  $NN$ - $\Delta N$  coupling in conventional nuclei, where the latter plays a very small role in binding few-nucleon systems since  $m_\Delta - m_N \sim 293$  MeV.

Another signal of the  $\Lambda N$ - $\Sigma N$  coupling probably comes from the observation that in  $S$ -wave relative states the  $\Lambda p$  interaction is more attractive than the  $\Lambda n$  interaction. This follows from a comparison of the experimental  $\Lambda$  binding energies for the ground states and the first excited states in the isospin  $I = 1/2$  doublet formed by  ${}^4_\Lambda\text{He}$  and  ${}^4_\Lambda\text{H}$ , (with separations of 0.35 MeV between the ground states and of 0.24 MeV for the excited states), which implies a relevant charge symmetry breaking for the  $\Lambda N$  interaction. Although this has been known for some decades, the issue has awakened interest in experimentalists [8] and theoreticians [9] in recent years. Despite the complete origin of the strong charge symmetry breaking in hypernuclei is still not known, one can safely say that a relevant contribution to it is given by the coupling between the  $\Lambda N$  and  $\Sigma N$  states, which turns out to be quite sensitive to the mass difference between the

initial and the final two-baryon states, thus preferring the process  $\Lambda p \rightarrow \Sigma^+ n$  ( $\Delta m \sim 75$  MeV) over the processes  $\Lambda p \rightarrow \Sigma^0 p$ ,  $\Lambda n \rightarrow \Sigma^0 n$  ( $\Delta m \sim 77$  MeV) and  $\Lambda n \rightarrow \Sigma^- p$  ( $\Delta m \sim 80.5$  MeV).

We also mention that the present status of the shell model fits to the experimental  $\Lambda$  energy levels in  $p$ -shell hypernuclei [10], the so called  $\gamma$ -ray data, show the need for alternative and/or improved descriptions of the  $\Lambda N$ - $\Sigma N$  coupling (see also the discussion of the first paper quoted in [1]). Finally, we remind the reader that also the deviations of the magnetic moments of  $\Lambda$  hypernuclei from the Schmidt values have been interpreted as a signal of the relevance of the  $\Lambda N$ - $\Sigma N$  coupling [11]. Despite these clues on the importance of the  $\Lambda N$ - $\Lambda\Sigma$  coupling in nuclear matter, the detailed  $\Sigma$  admixture properties in  $\Lambda$  hypernuclei and the  $\Sigma$  content and effects in compact stars are not known satisfactorily. It is an issue by which it is in principle possible to establish solid and prolific links between hypernuclei and compact stars.

We now return to the main topic of this contribution, i.e., the weak decay of  $\Lambda$  hypernuclei. We adopt a nuclear matter, many-body formalism extended to finite hypernuclei by the local density approximation (LDA), to describe the effects of the  $\Lambda N$ - $\Sigma N$  coupling on the nonmesonic weak decay of  ${}^{12}_\Lambda\text{C}$ ,  ${}^{28}_\Lambda\text{Si}$ ,  ${}^{56}_\Lambda\text{Fe}$ , and  ${}^{208}_\Lambda\text{Pb}$  hypernuclei. All isospin channels of the decays stimulated by one, two, or more nucleons can in principle be included in our diagrammatic approach. In the present paper, as a first step, we only consider explicitly the one-nucleon-induced channels  $\Lambda N \rightarrow nN$  and  $\Lambda N \rightarrow \Sigma N \rightarrow nN$ . However, a few considerations on the contribution of the two-nucleon-induced decay complement our discussion of the results. The adopted microscopic framework allowed us to demonstrate the importance of ground state contributions in one- and two-nucleon-induced decay processes [12]. In [13,14], the approach was applied to the calculation of the nucleon spectra emitted in the nonmesonic weak decay, while the three-nucleon-induced mode was studied for the first time in [15]. Finally, we recall that the same formalism was used to evaluate the nonmesonic decay widths for double- $\Lambda$  hypernuclei [16].

Only a few predictions are available on the  $\Lambda N \rightarrow \Sigma N \rightarrow nN$  decay mechanism [17–19]. Unfortunately, there are major disagreements among the predictions of these works, which adopted different approximation frameworks and potential models and considered different hypernuclei from the ones studied in the present paper: the ones in [17,18] deal with hypernuclei of the  $s$  shell, while the calculation in [19] is performed in nuclear matter, but without implementing the LDA. We perform some comparison with the latter approach in the “Results” section.

The paper is organized as follows. In Sec. II we present the theoretical formalism employed for the evaluation of the decay rates. In Sec. III the numerical results are discussed and compared with data. In Sec. IV we draw our conclusions. Finally, we relegate some technical details regarding the calculation of the decay rates to a few appendices.

## II. FORMALISM

Our main concern in the present contribution is the effect of the  $\Sigma$  baryon on the nonmesonic weak decay widths of

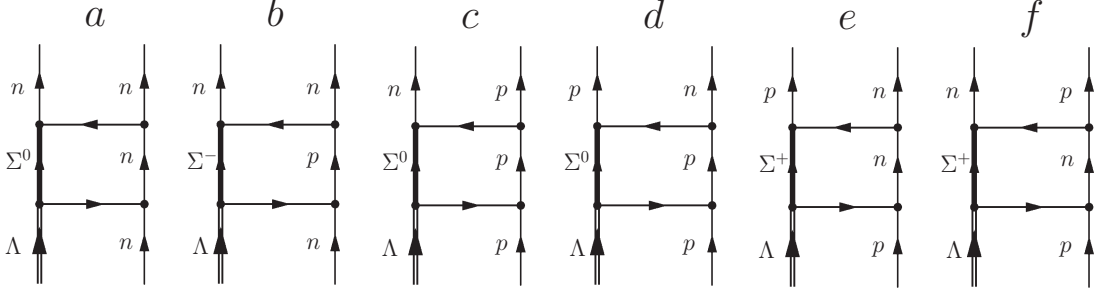


FIG. 1. The  $\Lambda N \rightarrow \Sigma N \rightarrow nN$  transition amplitudes originated by the  $\Lambda N$ - $\Sigma N$  coupling. Diagrams (a) and (b) [(c) to (f)] contribute to the neutron-induced (proton-induced) rate  $\Gamma_n$  ( $\Gamma_p$ ). In Appendix A we give the isospin wave functions for each contribution.

$\Lambda$  hypernuclei. Being heavier than the  $\Lambda$ , the  $\Sigma$  enters the problem through an intermediate, virtual  $\Sigma N$  two-baryon state: as we limit ourselves to one-nucleon-induced decays, the process  $\Lambda N \rightarrow \Sigma N \rightarrow nN$  has to be added to the customary one,  $\Lambda N \rightarrow nN$ .

Let us now introduce some generalities on the notation adopted for the decay widths. Limiting ourselves up to two-nucleon-stimulated decays, the total nonmesonic decay rate is given by

$$\Gamma_{\text{NM}} = \Gamma_1 + \Gamma_2, \quad (1)$$

where  $\Gamma_1$  and  $\Gamma_2$  denote the decay rates for the one-nucleon ( $\Lambda N \rightarrow nN$  and  $\Lambda N \rightarrow \Sigma N \rightarrow nN$ ) and the two-nucleon-stimulated decays ( $\Lambda NN \rightarrow nNN$  and  $\Lambda NN \rightarrow \Sigma NN \rightarrow nNN$ ) ( $N = n$  or  $p$ ). In terms of the various isospin channels, the one- and two-nucleon-induced rates are decomposed as

$$\Gamma_1 = \Gamma_n + \Gamma_p, \quad (2)$$

$$\Gamma_2 = \Gamma_{nn} + \Gamma_{np} + \Gamma_{pp}. \quad (3)$$

The subindices on the right-hand-side expressions indicate the initial (multi)nucleon state stimulating the weak decay:  $\Gamma_p \equiv \Gamma(\Lambda p \rightarrow np$  and  $\Lambda p \rightarrow \Sigma N \rightarrow np)$ , etc.

For the description of the decay rates we adopt a many-body technique, first introduced in [20], in which the calculation is performed in infinite nuclear matter and then it is extended to finite nuclei through the LDA. Let us then introduce the following schematic writing of the one-nucleon-stimulated decay width in nuclear matter:

$$\Gamma_1(\mathbf{k}, k_F) = \sum_f |\langle f | [V^{\Lambda N \rightarrow nN}(Q) + \mathcal{V}^{\Lambda N \rightarrow nN}(Q)] |0\rangle_{k_F}|^2 \delta(E_f - E_0), \quad (4)$$

where  $k = (k_0, \mathbf{k})$  stands for the  $\Lambda$  four-momentum inside infinite nuclear matter with Fermi momentum  $k_F$ , while  $|0\rangle_{k_F}$  and  $|f\rangle$  are the initial hypernuclear ground state (whose energy is  $E_0$ ) and the 2p-1h final state (with energy  $E_f$ ), respectively. Moreover,  $V^{\Lambda N \rightarrow nN}$  represents the meson-exchange weak transition potential adopted for the process  $\Lambda N \rightarrow nN$  ( $Q$  is the exchanged momentum) and is given later in the beginning of the next section. The effect of the  $\Sigma$  hyperon can be introduced by resorting to the following weak transition

potential:

$$\mathcal{V}^{\Lambda N \rightarrow nN}(Q) = \sum_{i, Q=q-p} V^{\Sigma N \rightarrow nN}(p) |i\rangle \frac{1}{E_i - E_0} \times \langle i | V^{\Lambda N \rightarrow \Sigma N}(q), \quad (5)$$

where the sum on the index  $i$  runs over the intermediate two-baryon configurations with energy  $E_i$  given by  $|\Sigma^0 n\rangle$ ,  $|\Sigma^0 p\rangle$ ,  $|\Sigma^- p\rangle$ , and  $|\Sigma^+ n\rangle$ . Expressions for the newly introduced meson-exchange transition potentials  $V^{\Sigma N \rightarrow nN}(p)$  and  $V^{\Lambda N \rightarrow \Sigma N}(q)$  are given soon. In Fig. 1 we show all the two-body transitions amplitudes involving the  $\Sigma$  and differentiating among the isospin channels which contribute to the one-nucleon-stimulated decay mechanism. Diagrams (a) and (b) contribute to  $\Gamma_n$ , while diagrams (c) to (f) contribute to  $\Gamma_p$ .

The rates for a finite hypernucleus are obtained from the ones in nuclear matter of Eq. (4) by the local density approximation [20], i.e., after averaging the nuclear matter widths over the  $\Lambda$  momentum distribution in the considered hypernucleus,  $|\tilde{\psi}_\Lambda(\mathbf{k})|^2$ , and over the local Fermi momentum,  $k_F(r) = \{3\pi^2 \rho(r)/2\}^{1/3}$ ,  $\rho(r)$  being the density profile of the hypernuclear core. From Eq. (4) one thus obtains

$$\Gamma_1 = \int d\mathbf{k} |\tilde{\psi}_\Lambda(\mathbf{k})|^2 \int d\mathbf{r} |\psi_\Lambda(\mathbf{r})|^2 \Gamma_1(\mathbf{k}, k_F(r)), \quad (6)$$

where for the wave function  $\psi_\Lambda(\mathbf{r})$  and its Fourier transform  $\tilde{\psi}_\Lambda(\mathbf{k})$  we adopt the  $1s_{1/2}$  harmonic oscillator wave function with frequency  $\hbar\omega$  adjusted to the experimental energy separation between the  $s$  and  $p$   $\Lambda$  levels in the hypernucleus. Specific values of  $\hbar\omega$  are reported in the ‘‘Results’’ section. The  $\Lambda$  total energy is given by  $k_0 = m_\Lambda + (\hbar\mathbf{k})^2/(2m_\Lambda) + B_\Lambda$ ,  $B_\Lambda$  being the  $\Lambda$  binding energy.

At this point it is convenient to step back in order to split Eq. (4) into three terms as follows:

$$\Gamma_1(\mathbf{k}, k_F) = \Gamma_1^0(\mathbf{k}, k_F) + \Delta\Gamma_1^{0\Sigma}(\mathbf{k}, k_F) + \Gamma_1^{\Sigma\Sigma}(\mathbf{k}, k_F), \quad (7)$$

where

$$\Gamma_1^0(\mathbf{k}, k_F) = \sum_f |\langle f | V^{\Lambda N \rightarrow nN}(Q) |0\rangle_{k_F}|^2 \delta(E_f - E_0), \quad (8)$$

$$\Delta\Gamma_1^{0\Sigma}(\mathbf{k}, k_F) = 2 \sum_{k_F} \langle 0 | (V^{\Lambda N \rightarrow nN}(Q))^\dagger \times |f\rangle \langle f | \mathcal{V}^{\Lambda N \rightarrow nN}(Q) |0\rangle_{k_F} \delta(E_f - E_0), \quad (9)$$

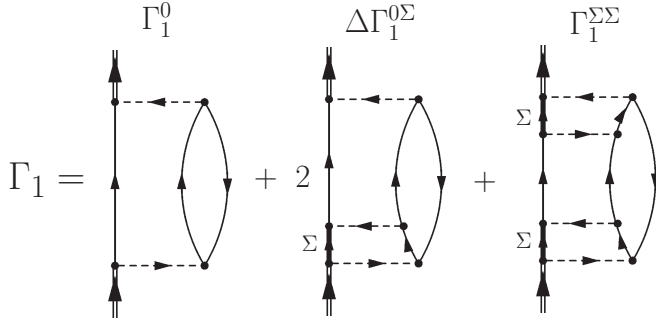


FIG. 2. Goldstone diagrams for the evaluation of the one-nucleon-stimulated decay rates in infinite nuclear matter once the  $\Lambda N$ - $\Sigma N$  strong coupling is taken into account.

$$\Gamma_1^{\Sigma\Sigma}(\mathbf{k}, k_F) = \sum_f |\langle f | \mathcal{V}^{\Lambda N \rightarrow nN}(Q) | 0 \rangle_{k_F}|^2 \delta(E_f - E_0). \quad (10)$$

Here, the  $\Gamma_1^0$  decay width corresponds to the usual one-body-induced decay process,  $\Lambda N \rightarrow nN$ . The effect of the  $\Sigma$  hyperon is contained in the two remaining terms:  $\Delta\Gamma_1^{0\Sigma}$ , which represents the interference between the  $\Lambda N \rightarrow nN$  and the  $\Lambda N \rightarrow \Sigma N \rightarrow nN$  amplitudes, and  $\Gamma_1^{\Sigma\Sigma}$ , which corresponds to the  $\Lambda N \rightarrow \Sigma N \rightarrow nN$  process. Goldstone diagrams for these three contributions are depicted in Fig. 2.

Let us then consider the expressions for the transition potentials. The weak transition potential  $\mathcal{V}^{YN \rightarrow nN}$ , with  $Y = \Lambda$  or  $\Sigma$ , and the strong interaction potential  $\mathcal{V}^{\Lambda N \rightarrow \Sigma N}$  read

$$\mathcal{V}^{YN \rightarrow nN(\Lambda N \rightarrow \Sigma N)}(t) = \sum_\tau \mathcal{O}_\tau \mathcal{V}_\tau^{YN \rightarrow nN(\Lambda N \rightarrow \Sigma N)}(t), \quad (11)$$

where the isospin dependence is given by

$$\mathcal{O}_\tau = \begin{cases} \mathbb{I} & \text{for } \tau = 0, \\ \boldsymbol{\tau}_1 \cdot \boldsymbol{\tau}_2 & \text{for } \tau = 1, \\ \mathbf{T}_1 \cdot \boldsymbol{\tau}_2 & \text{for } \tau = 2, \end{cases} \quad (12)$$

where  $\mathbb{I}$  represents the identity operator. Concerning the sum over  $\tau$  in Eq. (11), the values  $\tau = 0$  and 1 refer to the isoscalar and isovector parts of the interactions, respectively, while for  $\tau = 2$  we have introduced the  $I = 1/2$  to  $I = 3/2$  isospin transition operator  $\mathbf{T}$  needed by the  $\Sigma$  hyperon (details are given in Appendix A). The spin and momentum dependence

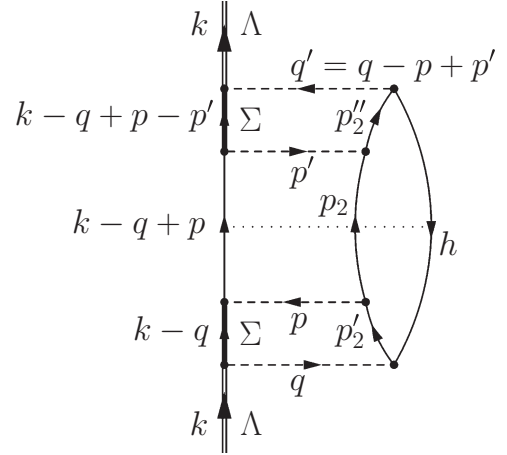


FIG. 3. Goldstone diagram contributing to  $\Gamma_1^{\Sigma\Sigma}$ . Concerning the values of the flowing energy-momenta, it is easy to see that  $p_2 = h + q - p$ ,  $p_2' = h + q - p + p'$ , and  $Q = q - p = q' - p'$ . In this diagram, the dotted line shows the final state.

of the weak transition potential is given by

$$\begin{aligned} \mathcal{V}_\tau^{YN \rightarrow nN}(t) = & (G_F m_\pi^2) [\mathcal{V}_{S,\tau}(t) \boldsymbol{\sigma}_1 \cdot \hat{\mathbf{t}} + \mathcal{V}_{S',\tau}(t) \boldsymbol{\sigma}_2 \cdot \hat{\mathbf{t}} \\ & + i\mathcal{V}_{Sv,\tau}(t) (\boldsymbol{\sigma}_1 \times \boldsymbol{\sigma}_2) \cdot \hat{\mathbf{t}} + \mathcal{V}_{C,\tau}(t) \\ & + \mathcal{V}_{\sigma,\tau}(t) (\boldsymbol{\sigma}_1 \cdot \boldsymbol{\sigma}_2) + \mathcal{V}_{L,\tau}(t) \boldsymbol{\sigma}_1 \cdot \hat{\mathbf{t}} \boldsymbol{\sigma}_2 \cdot \hat{\mathbf{t}}], \end{aligned} \quad (13)$$

where the functions  $\mathcal{V}_{S,\tau}(t)$ ,  $\mathcal{V}_{S',\tau}(t)$ ,  $\mathcal{V}_{Sv,\tau}(t)$ ,  $\mathcal{V}_{C,\tau}(t)$ ,  $\mathcal{V}_{\sigma,\tau}(t)$ , and  $\mathcal{V}_{L,\tau}(t)$ , which include short-range correlations, can be adjusted to reproduce any weak transition potential. Furthermore, the expression for the strong interaction potential is given by

$$\begin{aligned} \mathcal{V}_\tau^{\Lambda N \rightarrow \Sigma N}(t) = & \frac{f_\pi^2}{m_\pi^2} [\mathcal{U}_{C,\tau}(t) + \mathcal{U}_{\sigma,\tau}(t) (\boldsymbol{\sigma}_1 \cdot \boldsymbol{\sigma}_2) \\ & + \mathcal{U}_{L,\tau}(t) \boldsymbol{\sigma}_1 \cdot \hat{\mathbf{t}} \boldsymbol{\sigma}_2 \cdot \hat{\mathbf{t}}], \end{aligned} \quad (14)$$

where the functions  $\mathcal{U}_{C,\tau N}(t)$ ,  $\mathcal{U}_{\sigma,\tau N}(t)$ , and  $\mathcal{U}_{L,\tau N}(t)$  can also be adjusted to reproduce any strong interaction one wishes. The parametrizations chosen for the above weak and strong potential are discussed at the beginning of the next section.

We present now the explicit expression for  $\Gamma_1^{\Sigma\Sigma}(\mathbf{k}, k_F)$ , while we leave to Appendix C the case of  $\Delta\Gamma_1^{0\Sigma}(\mathbf{k}, k_F)$ . The expression of  $\Gamma_1^0(\mathbf{k}, k_F)$  can instead be found in [21]. In Fig. 3, we show the Goldstone diagram for  $\Gamma_1^{\Sigma\Sigma}$ , including the notation adopted for giving the energy-momentum for each line. By replacing the sum over momenta by integrals and by performing the energy integrations and the spin plus isospin summation in Eq. (10), the following expression is obtained:

$$\begin{aligned} \Gamma_{NN'}^{\Sigma\Sigma}(\mathbf{k}, k_F) = & \frac{1}{(2\pi)^{11}} (G_F m_\pi^2)^2 \left( \frac{f_\pi^2}{m_\pi^2} \right)^2 \iiint d\mathbf{q} d\mathbf{p} d\mathbf{p}' d\mathbf{h} \mathcal{W}_{NN'}^{\Sigma\Sigma}(q, p, p') \theta(|\mathbf{k} - \mathbf{q} + \mathbf{p}| - k_F) \theta(|\mathbf{h} + \mathbf{q}| - k_F) \\ & \times \theta(|\mathbf{h} + \mathbf{q} - \mathbf{p}| - k_F) \theta(|\mathbf{h} + \mathbf{q} - \mathbf{p} + \mathbf{p}'| - k_F) \theta(k_F - |\mathbf{h}|) \frac{1}{\Delta E_1(k, q, h)} \\ & \times \frac{1}{\Delta E_{1'}(k, q, h, p, p')} \delta(E_f(k, q, h, p) - E_i(k)), \end{aligned} \quad (15)$$

where  $\mathcal{W}_{NN}^{\Sigma\Sigma}(q, p, p')$  represents the spin plus isospin summation together with the momentum dependence of the different interactions (its expression is given in Appendix B). The energies entering the previous equation are

$$\begin{aligned} E_i(k) &= \varepsilon_\Lambda(|\mathbf{k}|) = k_0, \\ E_f(k, q, h, p) &= \varepsilon_N(|\mathbf{k} - \mathbf{q} + \mathbf{p}|) + \varepsilon_{N'}(|\mathbf{h} + \mathbf{q} - \mathbf{p}|) - \varepsilon_{N'}(|\mathbf{h}|), \\ \Delta E_1(k, q, h) &= [\varepsilon_\Sigma(|\mathbf{k} - \mathbf{q}|) + \varepsilon_N(|\mathbf{h} + \mathbf{q}|) - \varepsilon_{N'}(|\mathbf{h}|)] - \varepsilon_\Lambda(|\mathbf{k}|), \\ \Delta E_{1'}(k, q, h, p, p') &= [\varepsilon_\Sigma(|\mathbf{k} - \mathbf{q} + \mathbf{p} - \mathbf{p}'|) + \varepsilon_N(|\mathbf{h} + \mathbf{q} - \mathbf{p} + \mathbf{p}'|) - \varepsilon_{N'}(|\mathbf{h}|)] - \varepsilon_\Lambda(|\mathbf{k}|). \end{aligned}$$

Here, the generic single-particle energy reads  $\varepsilon_B(|\mathbf{t}|) = m_B + (\hbar\mathbf{t})^2/(2m_B) + B_B$ , where  $B_B$  stands for the binding energy of the baryon  $B = n, p$ , or  $\Sigma$ .

### III. RESULTS

All baryon-baryon interactions are described in terms of meson-exchange potentials: (1) the  $\Lambda N \rightarrow nN$  weak potential contains the exchange of the full set of mesons of the pseudoscalar ( $\pi, \eta, K$ ) and vector octets ( $\rho, \omega, K^*$ ), with strong coupling constants and cutoff parameters deduced from the Nijmegen soft-core interaction NSC97f [22] (for details on the weak transition potential we refer to [23]); (2) the  $\Lambda N \rightarrow \Sigma N$  strong potential includes the exchange of  $\pi$  and  $\rho$  mesons; (3) the  $\Sigma N \rightarrow nN$  weak potential includes the exchange of  $\pi$  and  $K$  mesons. For the novel potentials of the previous points (2) and (3) we provide in Tables I and II the strong and weak coupling constants adopted in the present calculation. For each of the mesons involved in these potentials, we have employed the same cutoff parameters as the ones in (1). At variance with the most studied  $\Lambda N \rightarrow nN$  weak potential, the current limited knowledge of both the weak and the strong interactions involving the  $\Sigma$  particle leads us to restrict to a  $\pi + \rho$  ( $\pi + K$ ) meson-exchange model for the  $\Lambda N \rightarrow \Sigma N$  strong interaction ( $\Sigma N \rightarrow nN$  weak interaction). Analyses of the  $\Sigma$ -hyperon formation spectra in the ( $K^-, \pi^\pm$ ) and ( $\pi^+, K^+$ ) reactions (see for instance [24]) showed that the  $\Sigma$ -nucleus potential has a substantial isospin dependence and, with the exception of very light systems, is repulsive:  $U_\Sigma = +(30 \pm 20)$  MeV at normal nuclear density. In the present calculation we always adopt the value  $B_\Sigma = +30$  MeV for the binding energy of the  $\Sigma$ . The  $\Lambda$  binding energies in the various hypernuclei are taken from experiment [25].

In Table III we give our results for the nonmesonic decay rates for  ${}^{12}_\Lambda\text{C}$  arising from the  $\Lambda N$ - $\Sigma N$  coupling for the neutron- and proton-induced channels,  $\Lambda n \rightarrow \Sigma N \rightarrow nn$  and

TABLE I. Nijmegen [26] strong coupling constants relevant for the transition amplitudes of Fig. 1.

Meson	Coupling
$\pi$	$g_{NN\pi} = 13.3$
	$g_{\Lambda\Sigma\pi} = 12.0$
$K$	$g_{\Sigma NK} = 4.28$
$\rho$	$g_{NN\rho}^V = 3.16$
	$g_{NN\rho}^T = 13.3$
	$g_{\Lambda\Sigma\rho}^V = 0$
	$g_{\Lambda\Sigma\rho}^T = 11.2$

$\Lambda p \rightarrow \Sigma N \rightarrow np$ , respectively (see the various contributions in Fig. 1). We remind the reader that the total neutron- and proton-induced rates are decomposed as  $\Gamma_n = \Gamma_n^0 + \Delta\Gamma_n^{0\Sigma} + \Gamma_n^{\Sigma\Sigma}$  and  $\Gamma_p = \Gamma_p^0 + \Delta\Gamma_p^{0\Sigma} + \Gamma_p^{\Sigma\Sigma}$ , respectively. The widths  $\Gamma_n^0$  and  $\Gamma_p^0$  refer to the  $\Lambda n \rightarrow nn$  and  $\Lambda p \rightarrow np$  processes, respectively, and are discussed later on. The results in Table III correspond to the cases of a weak  $\Sigma N \rightarrow nN$  potential modeled in terms of one-pion-exchange only (second line) and in terms of the exchange of pion plus  $K$  meson (third line). The interference terms show different behaviors:  $\Delta\Gamma_n^{0\Sigma}$  ( $\Delta\Gamma_p^{0\Sigma}$ ) provides a positive (negative) contribution to  $\Gamma_n$  ( $\Gamma_p$ ). Moreover, the  $\Gamma_n^{\Sigma\Sigma}$  and  $\Gamma_p^{\Sigma\Sigma}$  rates are more important than the interference contributions. Due to the peculiar interference effect, the overall contribution of the  $\Lambda N$ - $\Sigma N$  coupling is larger for the neutron-induced rate than for the proton-induced rate, thus increasing the value of the  $\Gamma_n/\Gamma_p$  ratio (we discuss this important ratio in the following). We also notice that the  $K$  exchange tends to increase both the  $\Sigma$ -driven decay rates, although its contribution is limited. This increase is at variance with the cases of the  $\Sigma$ -independent processes,  $\Lambda n \rightarrow nn$  and  $\Lambda p \rightarrow np$ , for which the  $K$  meson implies a reduction of both the corresponding rates  $\Gamma_n^0$  and  $\Gamma_p^0$ . This outcome is a simple consequence of the different relative sign between the  $K$ - and  $\pi$ -exchange potentials for the  $\Sigma$ -independent and the  $\Sigma$ -dependent processes.

In Table IV we report, again for  ${}^{12}_\Lambda\text{C}$ , the separate contributions of the parity-violating (PV) and the parity-conserving (PC) baryon-baryon transitions to the total decay rates,  $\Delta\Gamma_n^{0\Sigma} + \Gamma_n^{\Sigma\Sigma}$  and  $\Delta\Gamma_p^{0\Sigma} + \Gamma_p^{\Sigma\Sigma}$ , induced by the  $\Lambda N$ - $\Sigma N$  coupling. Results are given for the complete weak  $\Sigma N \rightarrow nN$

TABLE II. Parity-violating (PV) and parity-conserving (PC) weak coupling constants relevant for the transition amplitudes of Fig. 1. The  $\Sigma$  ( $K$ ) couplings were taken from [17] (second paper in [23]). The values are given in units of  $G_F m_\pi^2$ .

Vertex	PV ( $S$ wave)	PC ( $P$ wave)
$\Sigma^+ p \pi^0$	-1.45	-12.89
$\Sigma^+ n \pi^+$	0.04	-20.17
$\Sigma^- n \pi^-$	1.95	0.76
$\Sigma^0 n \pi^0$	1.00	-9.26
$\Sigma^0 p \pi^-$	1.45	12.89
$K^+ p n$	0.76	-23.70
$K^0 p p$	2.09	8.33
$K^0 n n$	2.85	-15.37

TABLE III. Contribution of the  $\Lambda N$ - $\Sigma N$  coupling to the neutron- and proton-induced weak decay rates of  ${}^{12}_{\Lambda}\text{C}$ ,  $\Lambda n \rightarrow \Sigma N \rightarrow nn$  and  $\Lambda p \rightarrow \Sigma N \rightarrow np$ . Two potential models for the weak  $\Sigma N \rightarrow nN$  processes are considered. The predictions are in units of the free  $\Lambda$  decay rate and we have used a frequency  $\hbar\omega = 11.00$  MeV, taken from [25], for the harmonic oscillator  $\Lambda$  wave function. See text for further details.

$V^{\Sigma N \rightarrow nN}$	$\Delta\Gamma_n^{0\Sigma}$	$\Gamma_n^{\Sigma\Sigma}$	$\Delta\Gamma_n^{0\Sigma} + \Gamma_n^{\Sigma\Sigma}$	$\Delta\Gamma_p^{0\Sigma}$	$\Gamma_p^{\Sigma\Sigma}$	$\Delta\Gamma_p^{0\Sigma} + \Gamma_p^{\Sigma\Sigma}$
$\pi$	0.010	0.018	0.020	-0.025	0.044	0.019
$\pi + K$	0.012	0.021	0.033	-0.029	0.051	0.022

potential model containing  $(\pi + K)$  exchange. Both for the neutron- and the proton-induced rates the PC terms are about five times larger than the PV ones. In contrast, it is a well established fact that for the customary  $\Lambda N \rightarrow nN$  decay the PC transitions only dominate in the case of proton-induced rates (the major contribution to the rate  $\Gamma_1^0 = \Gamma_n^0 + \Gamma_p^0$  is, however, given by the PV transition). The dominance of the neutron- and proton-induced PC rates exhibited in Table IV is explained as follows. The potential  $\mathcal{V}^{\Lambda N \rightarrow nN}(Q)$  describing the  $\Lambda N \rightarrow \Sigma N \rightarrow nN$  processes is build up from the strong  $V^{\Lambda N \rightarrow \Sigma N}(q)$  and the weak  $V^{\Sigma N \rightarrow nN}(p)$  potentials, as shown in Eq. (5) and Fig. 3. Concerning the four-momentum, for the  $\Lambda N \rightarrow \Sigma N \rightarrow nN$  transition one has  $Q = q - p = q' - p'$ , where  $p$  and  $p'$  (the four-momenta of the weak interaction lines, see Fig. 3) are independent of each other. The PV contribution to the  $\Sigma$ -driven decay rates is proportional to  $(\boldsymbol{\sigma} \cdot \hat{\boldsymbol{p}})(\boldsymbol{\sigma} \cdot \hat{\boldsymbol{p}}')$ ; for this term the spin summation provides  $\text{tr}(\boldsymbol{\sigma} \cdot \hat{\boldsymbol{p}} \boldsymbol{\sigma} \cdot \hat{\boldsymbol{p}}') = 2(\hat{\boldsymbol{p}} \cdot \hat{\boldsymbol{p}}')$ . Once integrated over the four-momentum variables, this spin summation, being a scalar product, is responsible for the significant reduction of the PV contributions to the  $\Lambda N \rightarrow \Sigma N \rightarrow nN$  rates, as shown in Table IV. It should be noted how the effect is due to the topology of the Goldstone diagram of Fig. 3, which contains two interaction lines and corresponds to decay processes involving the  $\Lambda N$ - $\Sigma N$  coupling.

The predictions for the neutron- and proton-induced decay rates,  $\Gamma_n = \Gamma_n^0 + \Delta\Gamma_n^{0\Sigma} + \Gamma_n^{\Sigma\Sigma}$  and  $\Gamma_p = \Gamma_p^0 + \Delta\Gamma_p^{0\Sigma} + \Gamma_p^{\Sigma\Sigma}$ , for  ${}^{12}_{\Lambda}\text{C}$  are shown in Table V together with the  $\Gamma_n/\Gamma_p$  ratio and the one-nucleon-induced rate,  $\Gamma_1 = \Gamma_n + \Gamma_p$ . The latest KEK [27] and FINUDA [28] data are also given for comparison. The second (third) column shows the results without (with) the inclusion of the  $\Lambda N$ - $\Sigma N$  coupling. The overall effect of this coupling is to increase  $\Gamma_n$  by about 23% and  $\Gamma_p$  by about 5%. The smaller variation for  $\Gamma_p$  is due to

TABLE IV. Parity-violating (PV) and parity-conserving (PC) contributions of the  $\Lambda N$ - $\Sigma N$  coupling to the neutron- and proton-induced weak decay rates of  ${}^{12}_{\Lambda}\text{C}$ . The full model for the weak  $\Sigma N \rightarrow nN$  potential, containing  $\pi$  and  $K$  exchange, is considered. The predictions are in units of the free  $\Lambda$  decay rate.

$(\Delta\Gamma^{0\Sigma} + \Gamma^{\Sigma\Sigma})_{\text{PV}}$	$(\Delta\Gamma^{0\Sigma} + \Gamma^{\Sigma\Sigma})_{\text{PC}}$	$(\Delta\Gamma^{0\Sigma} + \Gamma^{\Sigma\Sigma})_{\text{PV}}$	$(\Delta\Gamma^{0\Sigma} + \Gamma^{\Sigma\Sigma})_{\text{PC}}$
0.005	0.028	0.004	0.018

TABLE V. Predictions and recent data from KEK-E508 [27] and FINUDA [28] for the one-nucleon-stimulated nonmesonic weak decay widths of  ${}^{12}_{\Lambda}\text{C}$ . The results are in units of the free  $\Lambda$  decay rate.

Rate	Without $\Sigma$	With $\Sigma$	KEK-E508 [27]	KEK-FINUDA [28]
$\Gamma_n$	0.145	0.178	$0.23 \pm 0.08$	$0.28 \pm 0.12$
$\Gamma_p$	0.455	0.477	$0.45 \pm 0.10$	$0.493 \pm 0.088$
$\Gamma_1$	0.600	0.656	$0.68 \pm 0.13$	$0.78 \pm 0.09$
$\Gamma_n/\Gamma_p$	0.319	0.374	$0.51 \pm 0.14$	$0.58 \pm 0.27$

the previously discussed negative value of the interference rate  $\Delta\Gamma_p^{0\Sigma}$ . The  $\Gamma_n/\Gamma_p$  ratio thus increases, by about 17%, thanks to the implementation of the  $\Lambda N$ - $\Sigma N$  coupling.

A few details on the experiments are needed for a better understanding of the comparison with our results. The determinations listed as KEK-FINUDA have been reconstructed in the FINUDA paper [28] by starting from existing KEK data on  $\Gamma_p$  and the total ( $\Gamma_T$ ) and mesonic rates ( $\Gamma_M$ ), together with FINUDA data for  $\Gamma_p$  and the two-nucleon-induced decay rate,  $\Gamma_2$ . The KEK-FINUDA rate  $\Gamma_n$  ( $\Gamma_1$ ) is obtained as the difference  $\Gamma_n = \Gamma_T - \Gamma_M - \Gamma_p - \Gamma_2$  ( $\Gamma_1 = \Gamma_T - \Gamma_M - \Gamma_2$ ). Moreover, the KEK-FINUDA result for  $\Gamma_p$  is nothing but the weighted average between the KEK and FINUDA data. A rather good agreement of our final predictions (containing the  $\Lambda N$ - $\Sigma N$  coupling contribution) with the experiments is evident from Table V, especially as far as KEK data are considered (not considering the  $\Sigma$ -baryon effect would lead to predictions that are worse compared to the data). The differences with data are below the  $1\sigma$  level. In particular, notice that the prediction for the  $\Gamma_n/\Gamma_p$  ratio agrees with both KEK and KEK-FINUDA determinations only when the  $\Lambda N$ - $\Sigma N$  coupling is taken into account. The only discrepancy which exceeds, although moderately, the level of  $1\sigma$  concerns the KEK-FINUDA determination of  $\Gamma_1$ . This is related to the fact that our result for  $\Gamma_n$  underestimates the central value of the KEK-FINUDA determination, while a good agreement is evident concerning  $\Gamma_p$ .

In Table VI the final decay rates (including the effect of the  $\Lambda N$ - $\Sigma N$  coupling) predicted for a few hypernuclei over the periodic table are presented. We limit ourselves to consider those hypernuclei for which data are available for comparison. The  $\Lambda N$ - $\Sigma N$  coupling term,  $\Delta\Gamma_1^{0\Sigma} + \Gamma_1^{\Sigma\Sigma}$ , turns out to provide a contribution to the total one-nucleon-induced rate,  $\Gamma_1 = \Gamma_1^0 + \Delta\Gamma_1^{0\Sigma} + \Gamma_1^{\Sigma\Sigma}$ , of about 9% for all considered hypernuclei. The weight of the  $\Sigma$  hyperon is, however, more important for the  $\Gamma_n/\Gamma_p$  ratio: this ratio indeed increases by about 17% with respect to the  $\Sigma$ -independent prediction for all hypernuclei. The  $\Lambda N$ - $\Sigma N$  coupling improves the comparison with the experimental determinations of the  $\Gamma_n/\Gamma_p$  ratio in all cases. Note that the given percentage changes only slightly vary from  ${}^{12}_{\Lambda}\text{C}$  to  ${}^{208}_{\Lambda}\text{Pb}$ .

Consider now the one-nucleon-induced and the total non-mesonic widths,  $\Gamma_1$  and  $\Gamma_{\text{NM}} = \Gamma_1 + \Gamma_2$ . Only for  ${}^{12}_{\Lambda}\text{C}$  is a measurement of  $\Gamma_1$  available; we reproduce the KEK-E508 determination. For the rest of hypernuclei the only data at disposal refer to  $\Gamma_{\text{NM}}$ , which contain multinucleon-induced contributions. In particular, two-nucleon-stimulated decays are

TABLE VI. Decay rates predicted for various hypernuclei (in units of the free  $\Lambda$  decay rate). Experimental results for  $^{12}_{\Lambda}\text{C}$  are from KEK-E508 [27]; for  $^{28}_{\Lambda}\text{Si}$  and  $^{56}_{\Lambda}\text{Fe}$  they are from KEK-E307 [29]; finally, the datum for  $^{208}_{\Lambda}\text{Pb}$  is from COSY, Jülich [30]. The values for the harmonic oscillator frequencies are taken from [25], having employed  $\hbar\omega = 9.6, 8.0$  and  $4.4$  MeV for  $^{28}_{\Lambda}\text{Si}$ ,  $^{56}_{\Lambda}\text{Fe}$  and  $^{208}_{\Lambda}\text{Pb}$ , respectively.

Hypernucleus	$\Gamma_n$	$\Gamma_p$	$\Gamma_n/\Gamma_p$	$\Gamma_1$	$\Gamma_{\text{NM}}$	$(\Gamma_n/\Gamma_p)^{\text{Exp}}$	$\Gamma_1^{\text{Exp}}$	$\Gamma_{\text{NM}}^{\text{Exp}}$
$^{12}_{\Lambda}\text{C}$	0.18	0.48	0.37	0.66	0.88	$0.51 \pm 0.14$	$0.68 \pm 0.13$	$0.953 \pm 0.044$
$^{28}_{\Lambda}\text{Si}$	0.24	0.57	0.43	0.81	1.05	$0.53 \pm 0.28$		$1.125 \pm 0.125$
$^{56}_{\Lambda}\text{Fe}$	0.31	0.61	0.50	0.92	1.20	$0.87 \pm 0.29$		$1.21 \pm 0.08$
$^{208}_{\Lambda}\text{Pb}$	0.38	0.58	0.66	0.96	1.27			$1.82 \pm 0.14$

important: for all hypernuclei from  $^{12}_{\Lambda}\text{C}$  to  $^{208}_{\Lambda}\text{Pb}$ , we have shown (see the second paper of [12]) that the ratio  $\Gamma_2/\Gamma_1$  is rather mass independent, with the result  $\Gamma_2 \sim 0.3\Gamma_1$ . We expect that this prediction does not change much after adding the  $\Sigma$ -baryon contribution. Thus, from the present predictions for  $\Gamma_1$  we obtain the values for  $\Gamma_{\text{NM}} = \Gamma_1(1 + \Gamma_2/\Gamma_1)$  quoted in Table VI by adopting the predictions for  $\Gamma_2/\Gamma_1$  of the second paper of [12]. A good agreement with KEK-E307  $\Gamma_{\text{NM}}$  data is obtained for  $^{28}_{\Lambda}\text{Si}$  and  $^{56}_{\Lambda}\text{Fe}$ . This is not the case for  $^{208}_{\Lambda}\text{Pb}$ , where we largely underestimate the result obtained by the COSY Collaboration by averaging over measurements performed in the region of mass numbers  $A$  ranging from 180 and 220. A large overestimation is also seen if we consider older experimental determinations, with the exception of a CERN experiment of the 1980s, which, however, suffered from large error bars. The COSY datum is also difficult to reconcile with the nonmesonic decay rate measured by KEK-E307 for  $^{56}_{\Lambda}\text{Fe}$ : no known mechanism can be responsible for a large increase in the nonmesonic decay rate when going from  $^{56}_{\Lambda}\text{Fe}$  to the  $A \sim 200$  region. Such an increase contradicts the saturation property of the dominating  $\Lambda N \rightarrow nN$  interaction rate expected for increasing mass number and exhibited by all calculations to date; indeed, the range of the one-nucleon-induced process is consistently smaller than the radius of hypernuclei already in the region of  $^{56}_{\Lambda}\text{Fe}$ . Concerning the COSY datum, we have to note that, given the difficulty in employing direct timing methods for heavy hypernuclei, it has been obtained in experiments which measured the fission fragments—which are supposed to be generated by the nonmesonic decay—emitted by hypernuclei produced in proton-nucleus reactions. Large uncertainties affect such delayed fission experiments, because of the limited precision of the employed recoil shadow method: the produced hypernuclei cannot be unambiguously identified with this method. It is therefore not possible to exclude that mechanisms other than

TABLE VII. Decay rates for infinite nuclear matter extracted from Table XII in [19]. The widths are in units of the free  $\Lambda$  decay rate. The line “Without  $\Sigma$ ” (With  $\Sigma$ ) corresponds to the line “All-Tensor” (All- $\Sigma$ ) in the quoted table. For more details we refer the reader to the just mentioned work.

	$\Gamma_n$	$\Gamma_p$	$\Gamma_1$
Without $\Sigma$	0.38	1.64	2.02
With $\Sigma$	0.49	2.85	3.34

the nonmesonic decay (faster than the nonmesonic decay) contributed to hypernuclear fission in these experiments.

In reference to a comparison with other calculations, the one in [19] deserves attention as it is performed in nuclear matter. In this work, a partial wave expansion of the nuclear matter decay width is performed and the “ $s$ -wave approximation” is employed: the total angular momentum corresponding to the relative motion of the initial  $\Lambda N$  pair is taken equal to zero. The  $s$ -wave approximation is sometimes employed in finite nuclei calculations, for  $p$ -shell and heavier hypernuclei, although its applicability becomes increasingly questionable as the hypernuclear mass number increases. This work does not implement the LDA, and a nuclear matter Fermi momentum  $k_F = 270$  MeV/ $c$  is adopted. In addition, this approach replaces some momentum and angular variables by constant average values. We should also mention that the effect of the  $\Sigma$  hyperon on the decay width is implemented by a modified wave function, in which some average values are again employed. It is important to emphasize that, beyond the common use of nuclear matter, the formalism in [19] is different than ours. In Table VII we report some numerical results extracted from Table XII of [19]; they correspond to the case of the complete weak interaction potential. The alternatives without and with the contribution of the  $\Lambda N$ - $\Sigma N$  coupling are considered. The rather large values for  $\Gamma_1$  are attributed by the authors to the lack of strong nucleon-nucleon interactions in the final state in their approach.<sup>1</sup> We can compare the results of [19] of Table VII for nuclear matter with our predictions for the largest hypernucleus considered,  $^{208}_{\Lambda}\text{Pb}$ . With the incorporation of the  $\Sigma$ -hyperon effect, the rate  $\Gamma_n$  increases by  $\sim 29\%$  in [19], while we find an increase of  $\sim 23\%$ . Considering in addition the absolute rates, we can conclude that for the neutron-induced channel there is an acceptable agreement between our prediction and that of [19]. Instead, the big effect of the  $\Sigma$  on the rate  $\Gamma_p$  exhibited in [19] is not confirmed in our approach, as we find a  $\sim 5\%$  increase. The moderate variations of  $\Gamma_n$  and  $\Gamma_p$  obtained in the present work are consistent with the perturbative character inherent in the implementation of the  $\Lambda N$ - $\Sigma N$  coupling in our diagrammatic approach.

We conclude our discussion by an approximate interpretation of our predictions. It turns out that for all hypernuclei we considered in the present work the decay rates for the various

<sup>1</sup>Our definition of  $\Gamma_1$  is the one in Eq. (2), which is different from the one in [19].

$\Lambda N \rightarrow nN$  and  $\Lambda N \rightarrow \Sigma N \rightarrow nN$  processes satisfy, to a high degree of approximation, the following simple relations:

$$\begin{aligned} \frac{\Gamma_n^0}{\Gamma_p^0} &\sim 0.38 \frac{N}{Z}, \\ \frac{|\Delta\Gamma_n^{0\Sigma}|}{|\Delta\Gamma_p^{0\Sigma}|} &\sim \frac{\Gamma_n^{\Sigma\Sigma}}{\Gamma_p^{\Sigma\Sigma}} \sim 0.50 \frac{N}{Z}, \\ \frac{\Gamma_n}{\Gamma_p} &\equiv \frac{\Gamma_n^0 + \Delta\Gamma_n^{0\Sigma} + \Gamma_n^{\Sigma\Sigma}}{\Gamma_p^0 + \Delta\Gamma_p^{0\Sigma} + \Gamma_p^{\Sigma\Sigma}} \sim 0.45 \frac{N}{Z}, \end{aligned} \quad (16)$$

where  $N$  and  $Z$  denote the hypernuclear numbers of neutrons and protons, respectively. These outcomes naturally originate from the use of the local density approximation. An eventual finite nucleus calculation would modify some of the above neutron-to-proton ratios for particular hypernuclei while maintaining the general trend, proportional to  $N/Z$ . Due to the just discussed saturation property of the decay rates, to which we return in the next paragraph, the naive predictions of Eq. (16) do not mean that, separately,  $\Gamma_n^0$  is proportional to  $N$ ,  $\Gamma_p^0$  is proportional to  $Z$ , etc., up to the heaviest hypernuclei. This is only true for light hypernuclei, say up to  ${}^{12}_\Lambda\text{C}$ . What occurs is that the pairs of widths in each neutron-to-proton ratio separately saturate with increasing  $N$  and  $Z$  in such a way as to make these ratios proportional to  $N/Z$ .

This and other interesting points can be made easy to understand if one resorts to the qualitative description of the decay widths discussed in [31]. Let us consider the  $\Lambda N \rightarrow nN$  nonmesonic decay as a four-baryon pointlike interaction. In the semiclassical approximation one can then write the neutron- and proton-induced rates as follows:

$$\Gamma_{n(p)} = R_{n(p)} \int d\mathbf{r} |\psi_\Lambda(\mathbf{r})|^2 \rho_{n(p)}(\mathbf{r}), \quad (17)$$

where  $R_{n(p)}$  denote spin-averaged rates for the neutron-induced (proton-induced) process,  $|\psi_\Lambda(\mathbf{r})|$  is the  $\Lambda$  wave function (normalized to 1), and  $\rho_{n(p)}(\mathbf{r})$  the neutron and proton densities in the hypernucleus (normalized to  $N$  and  $Z$ , respectively) [31]. Note that the just introduced naive equations for  $\Gamma_n$  and  $\Gamma_p$  only consist of weighting the nucleon densities  $\rho_n(\mathbf{r})$  and  $\rho_p(\mathbf{r})$ , respectively, by the  $\Lambda$  wave function  $\psi_\Lambda(\mathbf{r})$ . As  $\rho_n(\mathbf{r}) = (N/A)\rho(\mathbf{r})$  and  $\rho_p(\mathbf{r}) = (Z/A)\rho(\mathbf{r})$ ,  $\rho(\mathbf{r})$  being the nuclear density, Eq. (17) provides

$$\Gamma_n = R_n \frac{N}{N+Z} \rho_A, \quad (18)$$

$$\Gamma_p = R_p \frac{Z}{N+Z} \rho_A, \quad (19)$$

$$\Gamma_n + \Gamma_p = (R_n + R_p) \rho_A, \quad (20)$$

in terms of the average nuclear density at the position of the  $\Lambda$  hyperon,  $\rho_A = \int d\mathbf{r} |\psi_\Lambda(\mathbf{r})|^2 \rho(\mathbf{r})$ . Note that this approximate reasoning can also be applied to all one-nucleon-induced rates discussed in the present paper, including the ones originating from the  $\Lambda N$ - $\Sigma N$  coupling. From the above approximate formulas one expects to obtain a saturation of  $\Gamma_n$  with  $N$ ,  $\Gamma_p$  with  $Z$ , and  $\Gamma_n + \Gamma_p$  with the mass number  $A = N + Z$ . However, the ratios  $N/(N+Z)$  and  $Z/(N+Z)$  display behaviors that are different from each other: due to

the particular  $N$  and  $Z$  values which correspond to existing hypernuclei, the former increases with  $N$  while the latter decreases with  $Z$ . According to this trend, by inspecting Eqs. (18) and (19) one would say that the proton-induced (neutron-induced) rate decreases (increases) for increasing  $A$ . However, the spin-averaged rates  $R_n$  and  $R_p$  provide themselves contributions to the decay rates, as indicated in Eqs. (18)–(20). Summarizing, the behavior exhibited by  $\Gamma_n$ ,  $\Gamma_p$  and  $\Gamma_n + \Gamma_p$  originates from the competition between two effects: the particular numbers of neutrons and protons and the spin-average for the neutron- and proton-stimulated decay processes. A net result is obtained in our complete numerical results: the decreasing of the proton-induced rates with  $Z$  is only seen by passing from  ${}^{56}_\Lambda\text{Fe}$  to  ${}^{208}_\Lambda\text{Pb}$ : all rates  $\Gamma_p^0$ ,  $\Delta\Gamma_p^{0\Sigma}$ , and  $\Gamma_p^{\Sigma\Sigma}$  for  ${}^{208}_\Lambda\text{Pb}$  are slightly smaller than the corresponding ones for  ${}^{56}_\Lambda\text{Fe}$ , as one can see in Table VI for the final rate  $\Gamma_p$ . On the other hand, from the same table it is evident that the rate  $\Gamma_1 = \Gamma_n + \Gamma_p$  is always an increasing and saturating function of  $A$ : this trend is justified in our exemplified discussion by the nuclear density at the  $\Lambda$  position  $\rho_A$  appearing in Eq. (20), which roughly counts the number of nucleon which, in a given hypernucleus, can stimulate one-nucleon-induced weak decays. Concluding, our schematic discussion of Eqs. (18) and (19) also provides

$$\frac{\Gamma_n}{\Gamma_p} = \frac{R_n}{R_p} \frac{N}{Z}, \quad (21)$$

which justifies the numerically obtained ratios of Eq. (16) with nearly constant values of  $R_n/R_p$ .

#### IV. CONCLUSIONS AND OUTLOOK

In the present contribution we have studied the effect of the  $\Lambda N$ - $\Sigma N$  strong coupling in the nonmesonic weak decay of  $\Lambda$  hypernuclei. This coupling introduces new decay channels,  $\Lambda N \rightarrow \Sigma N \rightarrow nN$ . A nuclear matter formalism has been adopted together with the local density approximation for calculations in hypernuclei ranging from  ${}^{12}_\Lambda\text{C}$  to  ${}^{208}_\Lambda\text{Pb}$ . The many-body content of the adopted diagrammatic approach is displayed in Fig. 1 for the decay amplitudes and Fig. 2 for the decay Goldstone diagrams. We have devoted particular attention to the one-nucleon-stimulated decay widths  $\Gamma_n = \Gamma_n^0 + \Delta\Gamma_n^{0\Sigma} + \Gamma_n^{\Sigma\Sigma}$  and  $\Gamma_p = \Gamma_p^0 + \Delta\Gamma_p^{0\Sigma} + \Gamma_p^{\Sigma\Sigma}$ .

As expected, the dominant contributions to the neutron- and proton-induced decay rates are the  $\Sigma$ -independent rates  $\Gamma_n^0$  and  $\Gamma_p^0$ . Moreover, the rates  $\Gamma_n^{\Sigma\Sigma}$  and  $\Gamma_p^{\Sigma\Sigma}$  turn out to be larger than the interference rates  $\Delta\Gamma_n^{0\Sigma}$  and  $\Delta\Gamma_p^{0\Sigma}$ . For  ${}^{12}_\Lambda\text{C}$  the total  $\Sigma$ -dependent rate  $\Delta\Gamma_n^{0\Sigma} + \Gamma_n^{\Sigma\Sigma}$  ( $\Delta\Gamma_p^{0\Sigma} + \Gamma_p^{\Sigma\Sigma}$ ) amounts to about 23% (5%) of the rate  $\Gamma_n$  ( $\Gamma_p$ ). The difference in the weights of the neutron- and proton-induced rates is due to a positive (negative) interference effect exhibited by  $\Delta\Gamma_n^{0\Sigma}$  ( $\Delta\Gamma_p^{0\Sigma}$ ). This outcome evidently leads to an increase of the  $\Gamma_n/\Gamma_p$  ratio. Concerning the total one-nucleon-induced rate,  $\Gamma_1 = \Gamma_n + \Gamma_p$ , it increases by about 9% as a result of the  $\Sigma N$ - $\Lambda N$  coupling. The  $\Gamma_n/\Gamma_p$  ratio instead increases by about 17%. For hypernuclei heavier than  ${}^{12}_\Lambda\text{C}$  the above percentages tend to slightly decrease with the mass number  $A$ . The parity-conserving part of the  $\Sigma$ -dependent rates dominate over the

parity-violating part by a factor of about 5 both for neutron- and proton-induced decays and for all hypernuclei.

For hypernuclei heavier than  ${}^{\Lambda}_{12}\text{C}$  only data for the nonmesonic rate  $\Gamma_{\text{NM}} = \Gamma_1 + \Gamma_2$  are available. Limiting ourselves to two-nucleon-stimulated decays, for all hypernuclei studied from  ${}^{\Lambda}_{12}\text{C}$  to  ${}^{208}_{\Lambda}\text{Pb}$  we have adopted here the predictions for the ratio  $\Gamma_2/\Gamma_1$  previously obtained in the second paper of [12] (one should also add that the ratio  $\Gamma_2/\Gamma_1$  is rather stable over all of the mass number range starting from  ${}^{\Lambda}_{12}\text{C}$ ; moreover, this ratio is expected to be only slightly varied by the inclusion of  $\Lambda N$ - $\Sigma N$  coupling dependent contributions). The nonmesonic rates were then obtained as  $\Gamma_{\text{NM}} = \Gamma_1(1 + \Gamma_2/\Gamma_1)$ , starting from present results for  $\Gamma_1$ . The predictions obtained in this way have the advantage of making comparison possible with the experimental determinations. The KEK and FINUDA data for the  $\Gamma_n/\Gamma_p$  ratio and the rates  $\Gamma_1$  and  $\Gamma_{\text{NM}}$  available for  ${}^{\Lambda}_{12}\text{C}$ ,  ${}^{\Lambda}_{28}\text{Si}$  and  ${}^{\Lambda}_{56}\text{Fe}$  have been reproduced rather well. The only exception is the case of the COSY measurement of the nonmesonic rate for  ${}^{208}_{\Lambda}\text{Pb}$ , which, however, is also impossible to reconcile with the KEK data for  ${}^{\Lambda}_{28}\text{Si}$  and  ${}^{\Lambda}_{56}\text{Fe}$  as far as the saturation mechanism of the decay rates is invoked.

Finally, we have also discussed an approximate interpretation of our numerical results, through the simple ratios of Eq. (16). The agreement of our calculations with these expressions shows that each individual neutron- and proton-stimulated decay rate separately saturates as a function of the neutron (proton) number  $N$  ( $Z$ ) in such a way as to make the various neutron-to-proton ratios proportional to  $N/Z$ . In particular, we have also explained how it is possible that the proton-induced rates  $\Gamma_p^0$ ,  $\Delta\Gamma_p^{0\Sigma}$ , and  $\Gamma_p^{\Sigma\Sigma}$  have the tendency, at a certain point, to decrease (instead of continuing to increase) with the mass of the hypernucleus.

The agreement among our final results and data is quite good and clearly demonstrates the necessity of including the effects of the  $\Lambda N$ - $\Sigma N$  strong coupling. Anyway, we believe that a refinement of the present microscopic approach can still be pursued. This improvement concerns the possible violation of the  $\Delta I = 1/2$  isospin rule in the one-nucleon-induced nonmesonic weak decay. Almost all calculations to date adopted meson-exchange models which only contain pure  $\Delta I = 1/2$  transitions. It is true that the quality of present data does not allow us to establish the degree of violation of the  $\Delta I = 1/2$  isospin rule in the one-nucleon-induced nonmesonic weak decay, but new theoretical hints could be of interest, especially for experimentalists. Without a resolution of this important question one will never be able to achieve the primary purpose of hypernuclear weak decay studies, which is to access the properties of baryon strangeness-changing processes such as  $\Lambda N \rightarrow nN$ .

We conclude with a brief review of the experiments scheduled for the future. An approved proposal at J-PARC consists of the E18 experiment [32]. It is designed to have much better statistics than KEK-E508 and concerns measurements of the rates  $\Gamma_n$ ,  $\Gamma_p$ , and  $\Gamma_2$  for  ${}^{\Lambda}_{11}\text{B}$  and  ${}^{\Lambda}_{12}\text{C}$ . Triple nucleon coincidence measurements could lead to (the first) direct measurements of  $\Gamma_2$  with a 10% statistical error. A second J-PARC approved experiment, E22 [33], consists of a high statistics study of the  $\Delta I = 1/2$  rule for  ${}^4_{\Lambda}\text{H}$  and  ${}^4_{\Lambda}\text{He}$ . An indication for the possibility of new experiments, which could

be performed at J-PARC by using the successful techniques developed by FINUDA, has been put forward in the last paper quoted in [3]. It consists of measurements of the full set of decay rates (including the total and the mesonic ones) for  ${}^5_{\Lambda}\text{He}$ ,  ${}^7_{\Lambda}\text{Li}$ ,  ${}^9_{\Lambda}\text{Be}$ ,  ${}^{11}_{\Lambda}\text{B}$ ,  ${}^{12}_{\Lambda}\text{C}$ ,  ${}^{15}_{\Lambda}\text{N}$ , and  ${}^{16}_{\Lambda}\text{O}$  with a statistical precision of  $\sim 5\%$ . We also remind the reader of the proposal in [34] for new measurements of the lifetimes and the proton-induced rates of  ${}^3_{\Lambda}\text{H}$ ,  ${}^4_{\Lambda}\text{H}$ ,  ${}^{12}_{\Lambda}\text{B}$  and other neutron-rich  $p$ -shell hypernuclei.

## ACKNOWLEDGMENT

This work was partially supported by CONICET, Argentina, under Contract No. PIP 00273.

## APPENDIX A: ISOSPIN SUMMATIONS

In this Appendix we develop isospin summation expressions for the decay rates  $\Gamma_1^{\Sigma\Sigma}$  and  $\Delta\Gamma_1^{0\Sigma}$ . For the hyperons  $\Lambda$  and  $\Sigma$ , having isospin 0 and 1, respectively, we adopt the isospin formalism. This consists in formally requesting isospin conservation at each weak baryonic vertex, i.e., in coupling the  $\Lambda$  and  $\Sigma$  hyperons into isospinors with isospin numbers  $I = 1/2$  and  $I_z = -1/2$ . The procedure is trivial for the  $\Lambda$ :  $|\Lambda\rangle = |0,0\rangle \otimes |1/2,-1/2\rangle = |1/2,-1/2\rangle$ . As far as the isospin quantum number is concerned, the  $\Lambda$  particle is thus modeled to behave as a neutron. For the  $\Sigma$  particle, the coupling to the isospinor runs as follows:

$$\begin{aligned} |\Sigma^0\rangle &= \frac{1}{\sqrt{3}} \left| \frac{1}{2}, -\frac{1}{2} \right\rangle + \sqrt{\frac{2}{3}} \left| \frac{3}{2}, -\frac{1}{2} \right\rangle, \\ |\Sigma^-\rangle &= \left| \frac{3}{2}, -\frac{3}{2} \right\rangle, \\ |\Sigma^+\rangle &= \sqrt{\frac{2}{3}} \left| \frac{1}{2}, \frac{1}{2} \right\rangle + \frac{1}{\sqrt{3}} \left| \frac{3}{2}, \frac{1}{2} \right\rangle. \end{aligned} \quad (\text{A1})$$

An inspection of Fig. 2, which shows the possible nonmesonic transitions amplitudes, leads to the following baryon-baryon isospin wave functions:

$$\begin{aligned} |nn\rangle &= \left| \frac{1}{2}, \frac{1}{2}, 1, -1 \right\rangle, \\ |np\rangle &= \frac{1}{\sqrt{2}} \left( \left| \frac{1}{2}, \frac{1}{2}, 1, 0 \right\rangle - \left| \frac{1}{2}, \frac{1}{2}, 0, 0 \right\rangle \right), \\ |pn\rangle &= \frac{1}{\sqrt{2}} \left( \left| \frac{1}{2}, \frac{1}{2}, 1, 0 \right\rangle + \left| \frac{1}{2}, \frac{1}{2}, 0, 0 \right\rangle \right), \\ |\Lambda n\rangle &= \left| \frac{1}{2}, \frac{1}{2}, 1, -1 \right\rangle, \\ |\Lambda p\rangle &= \frac{1}{\sqrt{2}} \left( \left| \frac{1}{2}, \frac{1}{2}, 1, 0 \right\rangle - \left| \frac{1}{2}, \frac{1}{2}, 0, 0 \right\rangle \right), \\ |\Sigma^0 n\rangle &= \frac{1}{\sqrt{3}} \left| \frac{1}{2}, \frac{1}{2}, 1, -1 \right\rangle + \sqrt{\frac{2}{3}} \left( \frac{\sqrt{3}}{2} \left| \frac{3}{2}, \frac{1}{2}, 2, -1 \right\rangle \right. \\ &\quad \left. + \frac{1}{2} \left| \frac{3}{2}, \frac{1}{2}, 1, -1 \right\rangle \right), \end{aligned}$$

$$\begin{aligned}
|\Sigma^0 p\rangle &= \frac{1}{\sqrt{6}} \left( \left| \frac{1}{2}, \frac{1}{2}, 1, 0 \right\rangle - \left| \frac{1}{2}, \frac{1}{2}, 0, 0 \right\rangle \right) \\
&\quad + \frac{1}{\sqrt{3}} \left( \left| \frac{3}{2}, \frac{1}{2}, 2, 0 \right\rangle - \left| \frac{3}{2}, \frac{1}{2}, 1, 0 \right\rangle \right), \\
|\Sigma^- p\rangle &= \frac{1}{2} \left( \left| \frac{3}{2}, \frac{1}{2}, 2, -1 \right\rangle - \sqrt{3} \left| \frac{3}{2}, \frac{1}{2}, 1, -1 \right\rangle \right), \\
|\Sigma^+ n\rangle &= \frac{1}{\sqrt{3}} \left( \left| \frac{1}{2}, \frac{1}{2}, 1, 0 \right\rangle + \left| \frac{1}{2}, \frac{1}{2}, 0, 0 \right\rangle \right) \\
&\quad + \frac{1}{\sqrt{6}} \left( \left| \frac{3}{2}, \frac{1}{2}, 2, 0 \right\rangle + \left| \frac{3}{2}, \frac{1}{2}, 1, 0 \right\rangle \right). \quad (\text{A2})
\end{aligned}$$

Let us start by considering the isospin summations for the particular case of a spin-independent weak interaction ( $\Sigma N \rightarrow NN$ ),

$$V(t) = V_0(t) + V_1(t) \boldsymbol{\tau}_1 \cdot \boldsymbol{\tau}_2 + V_2(t) \mathbf{T}_1 \cdot \boldsymbol{\tau}_2, \quad (\text{A3})$$

where  $t$  is the energy-momentum transferred by the interaction,  $\boldsymbol{\tau}$  denote the usual isospin-1/2 Pauli operators and  $\mathbf{T}$  the 1/2 to 3/2 isospin transition operators. For details on this operator we refer the reader to [35], where it is employed in connection with the  $\Delta(1232)$ -isobar particle. In a similar way and by making the substitution  $V \rightarrow U$  in Eq. (A3), we build up the strong interaction ( $\Lambda N \rightarrow \Sigma N$ ), having the same spin-isospin

dependence that  $V(t)$ . The next appendix is devoted to spin-dependent interactions and the relevant spin sums.

We can write down the different isospin amplitudes  $a$  to  $f$  depicted in Fig. 1 as

$$\begin{aligned}
\mathcal{A}_{(\Sigma^0 n)nn}(p, q) &= \langle nn | V(p) | \Sigma^0 n \rangle \langle \Sigma^0 n | U(q) | \Lambda n \rangle, \\
\mathcal{A}_{(\Sigma^- p)nn}(p, q) &= \langle nn | V(p) | \Sigma^- p \rangle \langle \Sigma^- p | U(q) | \Lambda n \rangle, \\
\mathcal{A}_{(\Sigma^0 p)np}(p, q) &= \langle np | V(p) | \Sigma^0 p \rangle \langle \Sigma^0 p | U(q) | \Lambda p \rangle, \\
\mathcal{A}_{(\Sigma^0 p)pn}(p, q) &= \langle pn | V(p) | \Sigma^0 p \rangle \langle \Sigma^0 p | U(q) | \Lambda p \rangle, \\
\mathcal{A}_{(\Sigma^+ n)pn}(p, q) &= \langle pn | V(p) | \Sigma^+ n \rangle \langle \Sigma^+ n | U(q) | \Lambda p \rangle, \\
\mathcal{A}_{(\Sigma^+ n)np}(p, q) &= \langle np | V(p) | \Sigma^+ n \rangle \langle \Sigma^+ n | U(q) | \Lambda p \rangle, \quad (\text{A4})
\end{aligned}$$

with  $\mathcal{A}_{(\Sigma^0 n)nn}(p, q)$  corresponding to the amplitude  $a$ , etc. Note that the notation for the amplitude is  $\mathcal{A}_{(int)f}(p, q)$ , where  $int$  is the intermediate configuration and  $f$  is the final state. We now replace the isospin wave functions by their explicit expressions from Eqs. (A2), and, using the values for the isospin matrix elements  $\langle 1/2, 1/2, 0, 0 | \boldsymbol{\tau}_1 \cdot \boldsymbol{\tau}_2 | 1/2, 1/2, 0, 0 \rangle = -3$ ,  $\langle 1/2, 1/2, 1, M_T | \boldsymbol{\tau}_1 \cdot \boldsymbol{\tau}_2 | 1/2, 1/2, 1, M_{T'} \rangle = \delta_{M_T, M_{T'}}$  and,  $\langle 1/2, 1/2, 1, M_T | \mathbf{T}_1 \cdot \boldsymbol{\tau}_2 | 3/2, 1/2, 1, M_{T'} \rangle = -4/\sqrt{6} \delta_{M_T, M_{T'}}$ , we get

$$\begin{aligned}
\mathcal{A}_{(\Sigma^0 n)nn}(p, q) &= \{3[V_0(p) + V_1(p)][U_0(q) + U_1(q)] + 4V_2(p)U_2(q)\}/9, \\
\mathcal{A}_{(\Sigma^- p)nn}(p, q) &= 2V_2(p)U_2(q), \\
\mathcal{A}_{(\Sigma^0 p)np}(p, q) &= \{3[V_0(p) - V_1(p)][U_0(q) - U_1(q)] + 4V_2(p)U_2(q)\}/9, \\
\mathcal{A}_{(\Sigma^0 p)pn}(p, q) &= \{6V_1(p)[U_0(q) - U_1(q)] + 4V_2(p)U_2(q)\}/9, \\
\mathcal{A}_{(\Sigma^+ n)pn}(p, q) &= \{12[(V_0(p) - V_1(p))U_1(q) + 2V_2(p)U_2(q)]\}/9, \\
\mathcal{A}_{(\Sigma^+ n)np}(p, q) &= [24V_1(p)U_1(q) + 2V_2(p)U_2(q)]/9. \quad (\text{A5})
\end{aligned}$$

For diagram  $\Gamma_1^{\Sigma\Sigma}$  (see Fig. 2) the isospin summations can be written as

$$\begin{aligned}
\mathcal{W}_{nn}^{\Sigma\Sigma}(q, p, p') &= [\mathcal{A}_{(\Sigma^- p)nn}(p', q') + \mathcal{A}_{(\Sigma^0 n)nn}(p', q')]^\dagger [\mathcal{A}_{(\Sigma^- p)nn}(p, q) + \mathcal{A}_{(\Sigma^0 n)nn}(p, q)], \\
\mathcal{W}_{np}^{\Sigma\Sigma}(q, p, p') &= [\mathcal{A}_{(\Sigma^+ n)np}(p', q') + \mathcal{A}_{(\Sigma^0 p)np}(p', q')]^\dagger [\mathcal{A}_{(\Sigma^+ n)np}(p, q) + \mathcal{A}_{(\Sigma^0 p)np}(p, q)], \\
\mathcal{W}_{pn}^{\Sigma\Sigma}(q, p, p') &= [\mathcal{A}_{(\Sigma^+ n)pn}(p', q') + \mathcal{A}_{(\Sigma^0 p)pn}(p', q')]^\dagger [\mathcal{A}_{(\Sigma^+ n)pn}(p, q) + \mathcal{A}_{(\Sigma^0 p)pn}(p, q)],
\end{aligned}$$

where  $q' = q - p + p'$  and the intermediate summations have been performed, up to this point, only for the isospin quantum number. Finally, using Eq. (A5) we have

$$\begin{aligned}
\mathcal{W}_{nn}^{\Sigma\Sigma}(q, p, p') &= \frac{1}{81} \{3[V_0(p) + V_1(p)]\{U_0(q) + U_1(q)\} + 22V_2(p)U_2(q)\} \\
&\quad \times \{3[V_0(p') + V_1(p')]\{U_0(q') + U_1(q')\} + 22V_2(p')U_2(q')\}, \\
\mathcal{W}_{np}^{\Sigma\Sigma}(q, p, p') &= \frac{1}{9} \{[V_0(p) - V_1(p)]U_0(q) + [-V_0(p) + 9V_1(p)]U_1(q) + 2V_2(p)U_2(q)\} \\
&\quad \times \{[V_0(p') - V_1(p')]\{U_0(q') + U_1(q')\} + 2V_2(p')U_2(q')\}, \\
\mathcal{W}_{pn}^{\Sigma\Sigma}(q, p, p') &= \frac{4}{9} \{V_1(p)U_0(q) + \{2V_0(p) - 3V_1(p)\}U_1(q) + V_2(p)U_2(q)\} \\
&\quad \times \{V_1(p')U_0(q') + \{2V_0(p') - 3V_1(p')\}U_1(q') + V_2(p')U_2(q')\}. \quad (\text{A6})
\end{aligned}$$

Following the same procedure for the diagram  $\Delta\Gamma_1^{0\Sigma}$  one gets

$$\begin{aligned}\mathcal{W}_{nn}^{0\Sigma}(q,p) &= \frac{1}{9}[3\{V_0(p) + V_1(p)\}\{U_0(q) + U_1(q)\} + 22V_2(p)U_2(q)][V_0(Q) + V_1(Q) + V_2(Q)], \\ \mathcal{W}_{np}^{0\Sigma}(q,p) &= \frac{1}{3}[\{V_0(p) - V_1(p)\}U_0(q) + \{-V_0(p) + 9V_1(p)\}U_1(q) + 2V_2(p)U_2(q)][V_0(Q) - V_1(Q) - V_2(Q)], \\ \mathcal{W}_{pn}^{0\Sigma}(q,p) &= \frac{4}{3}[V_1(p)U_0(q) + \{2V_0(p) - 3V_1(p)\}U_1(q) + V_2(p)U_2(q)][V_1(Q) + V_2(Q)],\end{aligned}\quad (\text{A7})$$

where  $Q = q - p$ .

### APPENDIX B: SPIN PLUS ISOSPIN SUMMATIONS FOR $\Gamma_1^{\Sigma\Sigma}$

In this Appendix we show the analytical expression of the function  $\mathcal{W}_{NN'}^{\Sigma\Sigma}(q,p,p')$ , which for convenience is expressed as

$$\mathcal{W}_{NN'}^{\Sigma\Sigma}(q,p,p') = \sum_{i,j,k,l} \mathcal{K}_{i,j,k,l}^{\Sigma\Sigma}(q,p,p')\mathcal{W}_{i,j,k,l}^{\Sigma\Sigma,NN'}(q,p,p'). \quad (\text{B1})$$

The functions  $\mathcal{W}_{i,j,k,l}^{\Sigma\Sigma,NN'}(q,p,p')$  contain the isospin summation [see Eq. (A6)] and are given by

$$\begin{aligned}\mathcal{W}_{i,j,k,l}^{\Sigma\Sigma,nn}(q,p,p') &= \frac{1}{81}[3\{\mathcal{V}_{j,0}(p) + \mathcal{V}_{j,1}(p)\}\{\mathcal{U}_{i,0}(q) + \mathcal{U}_{i,1}(q)\} + 22\mathcal{V}_{j,2}(p)\mathcal{U}_{i,2}(q)] \\ &\quad \times [3\{\mathcal{V}_{k,0}(p') + \mathcal{V}_{k,1}(p')\}\{\mathcal{U}_{i,0}(q') + \mathcal{U}_{i,1}(q')\} + 22\mathcal{V}_{k,2}(p')\mathcal{U}_{i,2}(q')], \\ \mathcal{W}_{i,j,k,l}^{\Sigma\Sigma,np}(q,p,p') &= \frac{1}{9}[\{\mathcal{V}_{j,0}(p) - \mathcal{V}_{j,1}(p)\}\mathcal{U}_{i,0}(q) + \{-\mathcal{V}_{j,0}(p) + 9\mathcal{V}_{j,1}(p)\}\mathcal{U}_{i,1}(q) + 2\mathcal{V}_{j,2}(p)\mathcal{U}_{i,2}(q)] \\ &\quad \times [\{\mathcal{V}_{k,0}(p') - \mathcal{V}_{k,1}(p')\}\mathcal{U}_{i,0}(q') + \{-\mathcal{V}_{k,0}(p') + 9\mathcal{V}_{k,1}(p')\}\mathcal{U}_{i,1}(q') + 2\mathcal{V}_{k,2}(p')\mathcal{U}_{i,2}(q')], \\ \mathcal{W}_{i,j,k,l}^{\Sigma\Sigma,pn}(q,p,p') &= \frac{4}{9}[\mathcal{V}_{j,1}(p)\mathcal{U}_{i,0}(q) + \{2\mathcal{V}_{j,0}(p) - 3\mathcal{V}_{j,1}(p)\}\mathcal{U}_{i,1}(q) + \mathcal{V}_{j,2}(p)\mathcal{U}_{i,2}(q)] \\ &\quad \times [\mathcal{V}_{k,1}(p')\mathcal{U}_{i,0}(q') + \{2\mathcal{V}_{k,0}(p') - 3\mathcal{V}_{k,1}(p')\}\mathcal{U}_{i,1}(q') + \mathcal{V}_{k,2}(p')\mathcal{U}_{i,2}(q')].\end{aligned}\quad (\text{B2})$$

In these expressions the  $\mathcal{V}$ 's and  $\mathcal{U}$ 's are taken from Eqs. (13) and (14), respectively, while the indices run as follows:  $\{i,l\} = C, \sigma$ , and  $L$  and  $\{j,k\} = C, \sigma, L, S, S'$ , and  $S_V$ . Finally, the spin summation is represented by the functions  $\mathcal{K}_{i,j,k,l}^{\Sigma\Sigma}(q,p,p')$ :

$$\begin{aligned}\mathcal{K}_{C,C,C,C}^{\Sigma\Sigma} &= \mathcal{K}_{C,C,L,\sigma}^{\Sigma\Sigma} = \mathcal{K}_{C,L,C,\sigma}^{\Sigma\Sigma} = \mathcal{K}_{L,C,C,\sigma}^{\Sigma\Sigma} = \mathcal{K}_{C,C,\sigma,L}^{\Sigma\Sigma} = \mathcal{K}_{C,\sigma,C,L}^{\Sigma\Sigma} = \mathcal{K}_{\sigma,C,C,L}^{\Sigma\Sigma} \\ &= \mathcal{K}_{C,L,\sigma,C}^{\Sigma\Sigma} = \mathcal{K}_{L,\sigma,C,C}^{\Sigma\Sigma} = \mathcal{K}_{C,\sigma,L,C}^{\Sigma\Sigma} = \mathcal{K}_{\sigma,L,C,C}^{\Sigma\Sigma} = \mathcal{K}_{C,S,S',\sigma}^{\Sigma\Sigma} = \mathcal{K}_{\sigma,S,S',C}^{\Sigma\Sigma} = 1, \\ \mathcal{K}_{C,C,\sigma,\sigma}^{\Sigma\Sigma} &= \mathcal{K}_{C,\sigma,\sigma,C}^{\Sigma\Sigma} = \mathcal{K}_{\sigma,\sigma,C,C}^{\Sigma\Sigma} = \mathcal{K}_{\sigma,C,C,\sigma}^{\Sigma\Sigma} = \mathcal{K}_{C,\sigma,C,\sigma}^{\Sigma\Sigma} = \mathcal{K}_{C,\sigma,C,\sigma}^{\Sigma\Sigma} = 3, \\ \mathcal{K}_{C,\sigma,\sigma,\sigma}^{\Sigma\Sigma} &= \mathcal{K}_{\sigma,C,\sigma,\sigma}^{\Sigma\Sigma} = \mathcal{K}_{\sigma,\sigma,C,\sigma}^{\Sigma\Sigma} = \mathcal{K}_{\sigma,\sigma,C,\sigma}^{\Sigma\Sigma} = -6, \\ \mathcal{K}_{\sigma,\sigma,\sigma,\sigma}^{\Sigma\Sigma} &= 21, \quad \mathcal{K}_{\sigma,\sigma,\sigma,L}^{\Sigma\Sigma} = \mathcal{K}_{\sigma,\sigma,L,\sigma}^{\Sigma\Sigma} = \mathcal{K}_{\sigma,L,\sigma,\sigma}^{\Sigma\Sigma} = \mathcal{K}_{L,\sigma,\sigma,\sigma}^{\Sigma\Sigma} = 7, \\ \mathcal{K}_{\sigma,\sigma,C,L}^{\Sigma\Sigma} &= \mathcal{K}_{C,\sigma,\sigma,L}^{\Sigma\Sigma} = \mathcal{K}_{\sigma,\sigma,L,C}^{\Sigma\Sigma} = \mathcal{K}_{\sigma,L,\sigma,C}^{\Sigma\Sigma} = \mathcal{K}_{L,\sigma,\sigma,C}^{\Sigma\Sigma} \\ &= \mathcal{K}_{\sigma,C,L,\sigma}^{\Sigma\Sigma} = \mathcal{K}_{C,L,\sigma,\sigma}^{\Sigma\Sigma} = \mathcal{K}_{\sigma,L,C,\sigma}^{\Sigma\Sigma} = \mathcal{K}_{L,C,\sigma,\sigma}^{\Sigma\Sigma} = \mathcal{K}_{\sigma,S,S',\sigma}^{\Sigma\Sigma} = -2, \\ \mathcal{K}_{C,C,L,L}^{\Sigma\Sigma} &= \mathcal{K}_{C,\sigma,L,L}^{\Sigma\Sigma} = \mathcal{K}_{\sigma,C,L,L}^{\Sigma\Sigma} = (\hat{\mathbf{p}}' \cdot \hat{\mathbf{q}}')^2, \\ \mathcal{K}_{C,L,L,C}^{\Sigma\Sigma} &= \mathcal{K}_{L,C,C,L}^{\Sigma\Sigma} = \mathcal{K}_{\sigma,L,L,C}^{\Sigma\Sigma} = \mathcal{K}_{C,L,L,\sigma}^{\Sigma\Sigma} = (\hat{\mathbf{p}} \cdot \hat{\mathbf{p}}')^2, \quad \mathcal{K}_{L,L,C,C}^{\Sigma\Sigma} = (\hat{\mathbf{q}} \cdot \hat{\mathbf{p}})^2, \quad \mathcal{K}_{L,C,L,C}^{\Sigma\Sigma} = (\hat{\mathbf{q}} \cdot \hat{\mathbf{p}}')^2, \\ \mathcal{K}_{C,L,C,L}^{\Sigma\Sigma} &= \mathcal{K}_{\sigma,L,C,L}^{\Sigma\Sigma} = \mathcal{K}_{C,L,\sigma,L}^{\Sigma\Sigma} = (\hat{\mathbf{p}} \cdot \hat{\mathbf{q}}')^2, \quad \mathcal{K}_{L,C,\sigma,L}^{\Sigma\Sigma} = \mathcal{K}_{L,\sigma,C,L}^{\Sigma\Sigma} = (\hat{\mathbf{q}} \cdot \hat{\mathbf{q}}')^2, \quad \mathcal{K}_{L,L,C,\sigma}^{\Sigma\Sigma} = \mathcal{K}_{L,L,\sigma,C}^{\Sigma\Sigma} = (\hat{\mathbf{q}} \cdot \hat{\mathbf{p}})^2, \\ \mathcal{K}_{C,L,L,L}^{\Sigma\Sigma} &= -[(\hat{\mathbf{q}}' \wedge \hat{\mathbf{p}}) \cdot \hat{\mathbf{p}}']^2, \quad \mathcal{K}_{L,C,L,L}^{\Sigma\Sigma} = -[(\hat{\mathbf{q}} \wedge \hat{\mathbf{q}}') \cdot \hat{\mathbf{p}}]^2, \\ \mathcal{K}_{L,L,C,L}^{\Sigma\Sigma} &= -[(\hat{\mathbf{q}} \wedge \hat{\mathbf{q}}') \cdot \hat{\mathbf{p}}]^2, \quad \mathcal{K}_{L,L,L,C}^{\Sigma\Sigma} = -[(\hat{\mathbf{q}} \wedge \hat{\mathbf{p}}') \cdot \hat{\mathbf{p}}]^2, \\ \mathcal{K}_{\sigma,\sigma,L,L}^{\Sigma\Sigma} &= [2 + (\hat{\mathbf{q}}' \cdot \hat{\mathbf{p}}')^2], \quad \mathcal{K}_{\sigma,L,L,\sigma}^{\Sigma\Sigma} = [2 + (\hat{\mathbf{p}} \cdot \hat{\mathbf{p}}')^2], \quad \mathcal{K}_{L,L,\sigma,\sigma}^{\Sigma\Sigma} = [2 + (\hat{\mathbf{p}} \cdot \hat{\mathbf{q}})^2], \\ \mathcal{K}_{L,\sigma,L,\sigma}^{\Sigma\Sigma} &= [2 + (\hat{\mathbf{q}} \cdot \hat{\mathbf{p}}')^2], \quad \mathcal{K}_{\sigma,L,\sigma,L}^{\Sigma\Sigma} = [2 + (\hat{\mathbf{q}}' \cdot \hat{\mathbf{p}})^2], \quad \mathcal{K}_{L,\sigma,\sigma,L}^{\Sigma\Sigma} = [2 + (\hat{\mathbf{q}} \cdot \hat{\mathbf{q}}')^2], \\ \mathcal{K}_{L,\sigma,L,L}^{\Sigma\Sigma} &= [(\hat{\mathbf{q}} \cdot \hat{\mathbf{q}}')^2 + (\hat{\mathbf{q}} \cdot \hat{\mathbf{p}}')^2 + (\hat{\mathbf{q}}' \cdot \hat{\mathbf{p}})^2 - 2(\hat{\mathbf{p}}' \cdot \hat{\mathbf{q}})(\hat{\mathbf{p}}' \cdot \hat{\mathbf{q}})(\hat{\mathbf{q}} \cdot \hat{\mathbf{q}}')], \\ \mathcal{K}_{\sigma,L,L,L}^{\Sigma\Sigma} &= [(\hat{\mathbf{p}} \cdot \hat{\mathbf{q}}')^2 + (\hat{\mathbf{p}} \cdot \hat{\mathbf{p}}')^2 + (\hat{\mathbf{p}}' \cdot \hat{\mathbf{q}})^2 - 2(\hat{\mathbf{p}} \cdot \hat{\mathbf{p}})(\hat{\mathbf{p}}' \cdot \hat{\mathbf{q}})(\hat{\mathbf{p}} \cdot \hat{\mathbf{q}}')], \\ \mathcal{K}_{C,\sigma,L,L}^{\Sigma\Sigma} &= \mathcal{K}_{\sigma,C,L,L}^{\Sigma\Sigma} = [-1 + (\hat{\mathbf{p}}' \cdot \hat{\mathbf{q}}')^2], \quad \mathcal{K}_{\sigma,L,C,L}^{\Sigma\Sigma} = \mathcal{K}_{C,L,\sigma,L}^{\Sigma\Sigma} = [-1 + (\hat{\mathbf{p}} \cdot \hat{\mathbf{q}}')^2],\end{aligned}$$



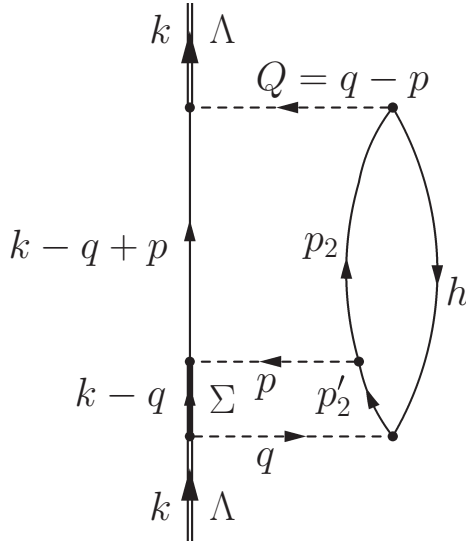


FIG. 4. Goldstone diagram corresponding to the interference rate  $\Delta\Gamma_1^{0\Sigma}$ . The energy-momentum transfer is shown along each line (note that  $p_2 = h + q - p$  and  $p'_2 = h + q$ ).

Finally we have,

$$\begin{aligned} \mathcal{K}_{C,C,C}^{0\Sigma} &= 1, \quad \mathcal{K}_{\sigma,\sigma,\sigma}^{0\Sigma} = -6, \quad \mathcal{K}_{C,\sigma,\sigma}^{0\Sigma} = \mathcal{K}_{\sigma,C,\sigma}^{0\Sigma} = \mathcal{K}_{\sigma,\sigma,C}^{0\Sigma} = 3, \\ \mathcal{K}_{\sigma,\sigma,L}^{0\Sigma} &= \mathcal{K}_{\sigma,L,\sigma}^{0\Sigma} = \mathcal{K}_{L,\sigma,\sigma}^{0\Sigma} = -2, \quad \mathcal{K}_{C,L,L}^{0\Sigma} = (\mathbf{p} \cdot \mathbf{q})^2, \\ \mathcal{K}_{L,C,L}^{0\Sigma} &= (\mathbf{Q} \cdot \mathbf{q})^2, \quad \mathcal{K}_{L,L,C}^{0\Sigma} = (\mathbf{Q} \cdot \mathbf{p})^2, \\ \mathcal{K}_{L,L,L}^{0\Sigma} &= -[(\mathbf{p} \wedge \mathbf{Q}) \cdot \mathbf{q}]^2, \quad \mathcal{K}_{\sigma,L,L}^{0\Sigma} = (-1 + (\mathbf{p} \cdot \mathbf{Q})^2), \\ \mathcal{K}_{L,\sigma,L}^{0\Sigma} &= (-1 + (\mathbf{q} \cdot \mathbf{Q})^2), \quad \mathcal{K}_{L,L,\sigma}^{0\Sigma} = (-1 + (\mathbf{p} \cdot \mathbf{q})^2), \\ \mathcal{K}_{C,S_v,S_v}^{0\Sigma} &= 2(\mathbf{Q} \cdot \mathbf{p}), \quad \mathcal{K}_{\sigma,S_v,S_v}^{0\Sigma} = -2(\mathbf{Q} \cdot \mathbf{p}), \\ \mathcal{K}_{L,S_v,S_v}^{0\Sigma} &= -2(\mathbf{Q} \cdot \mathbf{q})(\mathbf{p} \cdot \mathbf{q}), \quad \mathcal{K}_{C,S,S}^{0\Sigma} = \mathcal{K}_{C,S',S'}^{0\Sigma} = (\mathbf{p} \cdot \mathbf{Q}), \\ \mathcal{K}_{L,S,S}^{0\Sigma} &= \mathcal{K}_{L,S,S'}^{0\Sigma} = [-(\mathbf{Q} \cdot \mathbf{p}) + (\mathbf{p} \cdot \mathbf{q})(\mathbf{Q} \cdot \mathbf{q})], \\ \mathcal{K}_{L,S_v,S'}^{0\Sigma} &= \mathcal{K}_{L,S',S_v}^{0\Sigma} = (\mathbf{Q} \cdot \mathbf{p}) - (\mathbf{p} \cdot \mathbf{q})(\mathbf{Q} \cdot \mathbf{q}), \\ \mathcal{K}_{\sigma,S_v,S}^{0\Sigma} &= \mathcal{K}_{\sigma,S,S_v}^{0\Sigma} = -2(\mathbf{p} \cdot \mathbf{Q}), \\ \mathcal{K}_{\sigma,S,S'}^{0\Sigma} &= \mathcal{K}_{\sigma,S',S_v}^{0\Sigma} = 2(\mathbf{p} \cdot \mathbf{Q}), \quad \mathcal{K}_{\sigma,S,S'}^{0\Sigma} = \mathcal{K}_{\sigma,S',S}^{0\Sigma} = (\mathbf{p} \cdot \mathbf{Q}), \\ \mathcal{K}_{L,S,S'}^{0\Sigma} &= \mathcal{K}_{L,S',S}^{0\Sigma} = (\mathbf{Q} \cdot \mathbf{q})(\mathbf{p} \cdot \mathbf{q}), \end{aligned}$$

and  $\mathcal{K}_{i,j,k,l}^{0\Sigma} = 0$  otherwise.

- [1] E. Botta, T. Bressani, and G. Garbarino, *Eur. Phys. J. A* **48**, 41 (2012); A. Feliciello and T. Nagae, *Rept. Prog. Phys.* **78**, 096301 (2015).
- [2] J. Schaffner-Bielich, *Nucl. Phys. A* **835**, 279 (2010).
- [3] W. M. Alberico and G. Garbarino, *Phys. Rep.* **369**, 1 (2002); H. Outa *et al.*, *Nucl. Phys. A* **754**, 157c (2005); H. Outa, in *Hadron Physics*, Proceedings of the International School of Physics “E. Fermi”, Course CLVIII, edited by T. Bressani, A. Filippi and U. Wiedner (IOS Press, Amsterdam, 2005), p. 21; E. Botta, T. Bressani, S. Bufalino, and A. Feliciello, *Riv. Nuovo Cim.* **38**, 387 (2015).
- [4] Y. Akaishi, T. Harada, S. Shinmura, and K. S. Myint, *Phys. Rev. Lett.* **84**, 3539 (2000).
- [5] E. Hiyama, M. Kamimura, T. Motoba, T. Yamada, and Y. Yamamoto, *Phys. Rev. C* **65**, 011301 (2001); E. Hiyama and Yamada, *Prog. Part. Nucl. Phys.* **63**, 339 (2009).
- [6] A. Umeya and T. Harada, *Phys. Rev. C* **79**, 024315 (2009); **83**, 034310 (2011); A. Gal and D. J. Millener, *Phys. Lett. B* **725**, 445 (2013).
- [7] Y. Yamamoto, T. Furumoto, N. Yasutake, and Th. A. Rijken, *Phys. Rev. C* **90**, 045805 (2014); *Eur. Phys. J. A* **52**, 19 (2016).
- [8] T. O. Yamamoto *et al.* (J-PARC E13 Collaboration), *Phys. Rev. Lett.* **115**, 222501 (2015); T. Gogami *et al.* (HKS JLab E05-115 Collaboration), *Phys. Rev. C* **93**, 034314 (2016); F. Schulz *et al.* (A1 Collaboration), *Nucl. Phys. A* **954**, 149 (2016); E. Botta, T. Bressani, and A. Feliciello, *ibid.* **960**, 165 (2017).
- [9] A. Gal, *Phys. Lett. B* **744**, 352 (2015); D. Gazda and A. Gal, *Phys. Rev. Lett.* **116**, 122501 (2016); *Nucl. Phys. A* **954**, 161 (2016).
- [10] D. J. Millener, *Nucl. Phys. A* **881**, 298 (2012); **914**, 109 (2013).
- [11] C. B. Dover, H. Feshbach, and A. Gal, *Phys. Rev. C* **51**, 541 (1995); K. Saito, M. Oka, and T. Suzuki, *Nucl. Phys. A* **625**, 95 (1997).
- [12] E. Bauer and G. Garbarino, *Nucl. Phys. A* **828**, 29 (2009); *Phys. Rev. C* **81**, 064315 (2010).
- [13] E. Bauer, G. Garbarino, A. Parreno, and A. Ramos, *Nucl. Phys. A* **836**, 199 (2010).
- [14] E. Bauer and G. Garbarino, *Phys. Lett. B* **698**, 306 (2011); **716**, 249 (2012).
- [15] E. Bauer, G. Garbarino, and C. A. Rodríguez Peña, *Phys. Lett. B* **766**, 144 (2017).
- [16] E. Bauer, G. Garbarino, and C. A. Rodríguez Peña, *Phys. Rev. C* **92**, 014301 (2015).
- [17] H. Bando, Y. Shono, and H. Takaki, *Int. J. Mod. Phys. A* **3**, 1581 (1988).
- [18] K. Sasaki, T. Inoue, and M. Oka, *Nucl. Phys. A* **707**, 477 (2002).
- [19] N. J. Robertson and W. H. Dickhoff, *Phys. Rev. C* **72**, 024320 (2005).
- [20] E. Oset and L. L. Salcedo, *Nucl. Phys. A* **443**, 704 (1985).
- [21] E. Bauer and F. Krmptić, *Nucl. Phys. A* **717**, 217 (2003).
- [22] Th. A. Rijken, V. G. J. Stoks, and Y. Yamamoto, *Phys. Rev. C* **59**, 21 (1999); V. G. J. Stoks and Th. A. Rijken, *ibid.* **59**, 3009 (1999).
- [23] A. Parreño, A. Ramos, and C. Bennhold, *Phys. Rev. C* **56**, 339 (1997); **65**, 015205 (2001).
- [24] J. Dabrowski and J. Rozynek, *Phys. Rev. C* **78**, 037601 (2008).
- [25] O. Hashimoto and H. Tamura, *Prog. Part. Nucl. Phys.* **57**, 564 (2006).
- [26] M. N. Nagels, T. A. Rijken, and J. J. de Swart, *Phys. Rev. D* **15**, 2547 (1977); P. M. M. Maessen, T. A. Rijken, and J. J. de Swart, *Phys. Rev. C* **40**, 2226 (1989).
- [27] M. Kim, S. Ajimura, K. Aoki, A. Banu, H. Bhang, T. Fukuda, O. Hashimoto, J. I. Hwang, S. Kameoka, B. H. Kang, E. Kim, J. H. Kim, T. Maruta, Y. Miura, Y. Miyake, T. Nagae, M. Nakamura, S. N. Nakamura, H. Noumi, S. Okada, Y. Okayasu, H. Outa, H. Park, P. K. Saha, Y. Sato, M. Sekimoto, T. Takahashi, H. Tamura,

- K. Tanida, A. Toyoda, K. Tshoo, K. Tsukada, T. Watanabe, and H. J. Yim, *Phys. Rev. Lett.* **103**, 182502 (2009); H. Bhang *et al.*, *J. Kor. Phys. Soc.* **59**, 1461 (2011).
- [28] E. Botta, T. Bressani, S. Bufalino, and A. Feliciello, *Phys. Lett. B* **748**, 86 (2015).
- [29] Y. Sato, S. Ajimura, K. Aoki, H. Bhang, T. Hasegawa, O. Hashimoto, H. Hotchi, Y. D. Kim, T. Kishimoto, K. Maeda, H. Noumi, Y. Ohta, K. Omata, H. Outa, H. Park, M. Sekimoto, T. Shibata, T. Takahashi, and M. Youn, *Phys. Rev. C* **71**, 025203 (2005).
- [30] W. Cassing *et al.*, *Eur. Phys. J. A* **16**, 549 (2003).
- [31] W. M. Alberico and G. Garbarino, *Phys. Lett. B* **486**, 362 (2000).
- [32] H. Bhang *et al.*, Letter of intent for the E18 experiment at J-PARC, 2006 (unpublished); M. Kim *et al.*, *Nucl. Phys. A* **835**, 434 (2010).
- [33] S. Ajimura *et al.*, Letter of intent for the E22 experiment at J-PARC, 2007 (unpublished).
- [34] M. Agnello, E. Botta, T. Bressani, S. Bufalino, and A. Feliciello, *Nucl. Phys. A* **954**, 176 (2016).
- [35] G. E. Brown and W. Weise, *Phys. Rep.* **22**, 279 (1975).